JBC RESEARCH ARTICLE

DEAD box 1 (DDX1) protein binds to and protects cytoplasmic stress response mRNAs in cells exposed to oxidative stress

Received for publication, February 5, 2022, and in revised form, June 13, 2022 Published, Papers in Press, June 23, 2022,
https://doi.org/10.1016/j.jbc.2022.102180

Lei Li[1,‡], **Mansi Garg**[1,‡], **Yixiong Wang**[1], **Weiwei Wang**[2], **and Roseline Godbout**[1,*]

From the [1]*Department of Oncology, Cross Cancer Institute, and* [2]*Department of Medicine, University of Alberta, Edmonton, Alberta, Canada*

Edited by Ronald Wek

The integrated stress response is a network of highly orchestrated pathways activated when cells are exposed to environmental stressors. While global repression of translation is a well-recognized hallmark of the integrated stress response, less is known about the regulation of mRNA stability during stress. DEAD box proteins are a family of RNA unwinding/remodeling enzymes involved in every aspect of RNA metabolism. We previously showed that DEAD box 1 (DDX1) protein accumulates at DNA double-strand breaks during genotoxic stress and promotes DNA double-strand break repair *via* homologous recombination. Here, we examine the role of DDX1 in response to environmental stress. We show that DDX1 is recruited to stress granules (SGs) in cells exposed to a variety of environmental stressors, including arsenite, hydrogen peroxide, and thapsigargin. We also show that DDX1 depletion delays resolution of arsenite-induced SGs. Using RNA immunoprecipitation sequencing, we identify RNA targets bound to endogenous DDX1, including RNAs transcribed from genes previously implicated in stress responses. We show the amount of target RNAs bound to DDX1 increases when cells are exposed to stress, and the overall levels of these RNAs are increased during stress in a DDX1-dependent manner. Even though DDX1's RNA-binding property is critical for maintenance of its target mRNA levels, we found RNA binding is not required for localization of DDX1 to SGs. Furthermore, DDX1 knockdown does not appear to affect RNA localization to SGs. Taken together, our results reveal a novel role for DDX1 in maintaining cytoplasmic mRNA levels in cells exposed to oxidative stress.

Eukaryotic cells are routinely exposed to a variety of stressors, from genotoxic stress such as ultraviolet radiation and ionizing radiation (IR) to environmental stress including oxidizing agents and heat shock. Organisms have evolved different mechanisms to minimize cell damage and maximize cell survival when exposed to stress. For example, the DNA damage response pathway is activated immediately after DNA double-strand break (DSB) formation (1), whereas stress granule (SG) formation is rapidly induced upon oxidative stimuli or endoplasmic reticulum stress (2). SGs are membrane-less structures that form in the cytoplasm through liquid–liquid phase separation (3, 4). SGs consist of dense stable cores and more dynamic shells that surround the cores (5). Components of SGs include mRNAs, translation initiation factors, 40S ribosomal subunits, and RNA-binding proteins that regulate mRNA translation, stability, and other aspects of RNA metabolism. SG formation is a reversible process (3, 4). Abnormalities in SG assembly and disassembly have been implicated in many neurodegenerative diseases (6, 7).

SG formation is an important part of the elaborate signaling network called integrated stress response (ISR), which is activated when cells are exposed to various forms of environmental stress (8). The key feature of ISR is the suppression of global translation in order to preserve energy for cellular adaptation during stress. In eukaryotes, the central player in this stress-induced translational inhibition is the initiation factor eIF2α. eIF2α is rapidly phosphorylated by different kinases depending on the type of stress (9). Phosphorylated eIF2α inhibits eIF2B, the nucleotide exchange factor that converts eIF2-GDP to eIF2-GTP, and limits translation initiation, resulting in the repression of global translation (10). However, eIF2α phosphorylation also promotes translation of select genes such as the transcriptional activators *ATF4* and *ATF5* which in turn promote stress adaptation and cell survival (8). Although eIF2α phosphorylation usually triggers SG formation, SG can also be induced by other translation initiation inhibitors without eliciting eIF2α phosphorylation (11).

In addition to inhibition of mRNA translation, ISR also involves regulation of mRNA stability under stress conditions. SGs are evolutionally conserved structures that are induced by a broad spectrum of environmental stresses. As such, SGs have been proposed to protect mRNAs from degradation during stress (12), largely based on the findings that SGs contain proteins that recruit mRNAs (13–15) and stabilize mRNAs (14, 16). Consistent with a role in RNA protection, some types of SG-inducing stressors also inhibit mRNA deadenylation (17, 18), a process that precedes the degradation of most

‡ These authors contributed equally to this work.
* For correspondence: Roseline Godbout, rgodbout@ualberta.ca.
Present address for Weiwei Wang: Geneis Inc, Building A, 5 Guangshun North Street, Beijing, China.

mRNAs. However, more recent studies reveal that impaired SG assembly does not influence the stability of bulk mRNA during stress in both yeast and mammalian cells (19, 20). In addition, whether mRNAs reside within SGs or remain in the cytosol during stress has little effect on mRNA translation and degradation when cells recover from stress (21, 22). Regardless of their exact location, mRNAs have been reported to be stabilized in response to environmental stress (17, 18, 23).

DEAD box proteins are a family of RNA unwinding/remodeling proteins that function in all aspects of RNA metabolism, from transcription to RNA transport and RNA decay (24). The *DDX1* (DEAD box 1) gene is ubiquitously expressed in mammalian tissues and essential for early embryonic development. Homozygous knockout of mouse *Ddx1* leads to embryonic lethality prior to the blastocyst stage (25, 26). Although viable, *Ddx1* knockout flies are smaller than their wildtype counterparts, and their fertility is severely impaired (27). In humans, *DDX1* is amplified and overexpressed in a subset of retinoblastoma and neuroblastoma (NB) tumors and cell lines (28, 29). In breast cancer, high levels of DDX1 correlate with a poor prognosis (30). More recently, mutations in *DDX1* have been associated with primary microcephaly in children (31).

DDX1 is a functionally versatile protein with reported roles in DNA DSB repair (32–34), RNA transport and localized translation in neurons (35, 36), regulation of R-loop formation (37), tRNA splicing (38), rRNA biogenesis (39) and translational control (40). DDX1 can bind to single and double stranded RNAs, G-quadruplex RNAs, and RNA–DNA duplexes *in vitro* (33, 37, 41). Proteomic analysis of SG components indicates that DDX1 is located in the SG core (5), with a number of studies showing DDX1 colocalization with SG markers after heat shock and oxidative stress (42–44). However, these reports do not address the role of DDX1 in the cellular response to environmental stress. Here, we investigate the localization of DDX1 in cells exposed to different types of environmental stressors in cancer cell lines. We use DDX1 RNA immunoprecipitation (RIP) followed by next-generation sequencing and quantitative RT-PCR (RT-qPCR) analysis to identify targets of endogenous DDX1. We show that DDX1 promotes maintenance of target mRNA levels during oxidative stress. We also show that DDX1's RNA-binding activity is critical to this activity but dispensable for localization of DDX1 to SGs. Given DDX1's previously documented role in promoting DNA DSB repair under genotoxic stress (32–34), we propose an equally important role for DDX1 in environmental stress responses through mRNA protection.

Results

Localization of DDX1 in SGs

We have previously reported that following treatment with genotoxic agents such as IR and bleomycin, DDX1 quickly accumulates at DNA DSBs (32–34). Other laboratories have shown that when cells are treated with arsenite, which induces an oxidative stress response, both overexpressed and endogenous DDX1 colocalize with SG markers such as G3BP1 and YB1 in the cytoplasm (42–44). To investigate whether DDX1 localizes to SGs as a general response to environmental stress, we treated U2OS cells with arsenite, H_2O_2 (oxidative stress), heat shock, thapsigargin (ER stress), or MG132 (proteasome stress). Cells were coimmunostained with anti-DDX1 and either anti-TIA1 or anti-G3BP1 antibodies, both of which are well-recognized SG markers. In all cases, DDX1 colocalized with SG markers (Figs. 1 and S1). We also found that DDX1 localizes to SGs in response to environmental stress in cell lines other than U2OS, including HeLa (cervical cancer), BE(2)-C (NB), and human embryonic kidney HEK 293 (Fig. 1) using TIA1 as a marker. Similar results were observed in GM38 (normal fibroblasts) (data not shown). In contrast, no cytoplasmic DDX1 aggregation was observed under non-stressed conditions (Fig. 1). Therefore, localization of DDX1 to SGs appears to be a general cellular response to environmental stress.

Roles of DDX1 in SG disassembly

Some SG components such as G3BP1 and TDP-43 contribute to SG assembly (45). To examine whether DDX1 plays a role in SG assembly, we depleted DDX1 in U2OS cells using DDX1-specific siRNAs (Fig. S2). Control (scrambled siRNA-transfected) and DDX1-depleted U2OS cells were treated with 0.5 mM arsenite, and SGs were analyzed 20, 30, and 45 min later. Our results show that DDX1 depletion does not affect arsenite-induced SG assembly based on the percentage of cells that are positive for SGs as well as the average number of SGs per cell (anti-TIA1 immunostaining) (Fig. 2, *A* and *B*).

SGs gradually resolve after environmental stressors are removed (3). We next examined the effects of DDX1 on SG resolution. Control and DDX1-depleted U2OS cells were treated with 0.5 mM arsenite for 45 min, washed with pre-warmed PBS, and the medium replaced. SG analysis was carried out 90 min and 120 min after medium replacement. After 90 min recovery, ∼70% of control cells remained positive for SG immunostaining, in contrast to ∼90% of DDX1-depleted cells (Fig. 2, *C* and *D*). Similarly, after 120 min of recovery, ∼10% of control cells retained SGs, in contrast to ∼20% of DDX1-depleted cells. In addition, at both time points, the average SG numbers per cell were ∼2- to 3-fold higher in DDX1-depleted cells compared to control cells (Fig. 2, *C* and *D*).

A hallmark of ISR is phosphorylation of the translation initiation factor eIF2α. Phosphorylation of eIF2α blocks the exchange of eIF2-GDP to eIF2-GTP and limits translation initiation, which in turn represses global translation (10). eIF2α phosphorylation and dephosphorylation coincide with SG formation and clearance, respectively (8). To examine whether DDX1 plays a role in regulating eIF2α phosphorylation and dephosphorylation, we analyzed eIF2α phosphorylation status in control and DDX1-depleted U2OS cells during stress and recovery. We did not notice any appreciable difference in eIF2α phosphorylation status as the result of DDX1 depletion (Fig. S3). Taken together, our results suggest that DDX1 plays

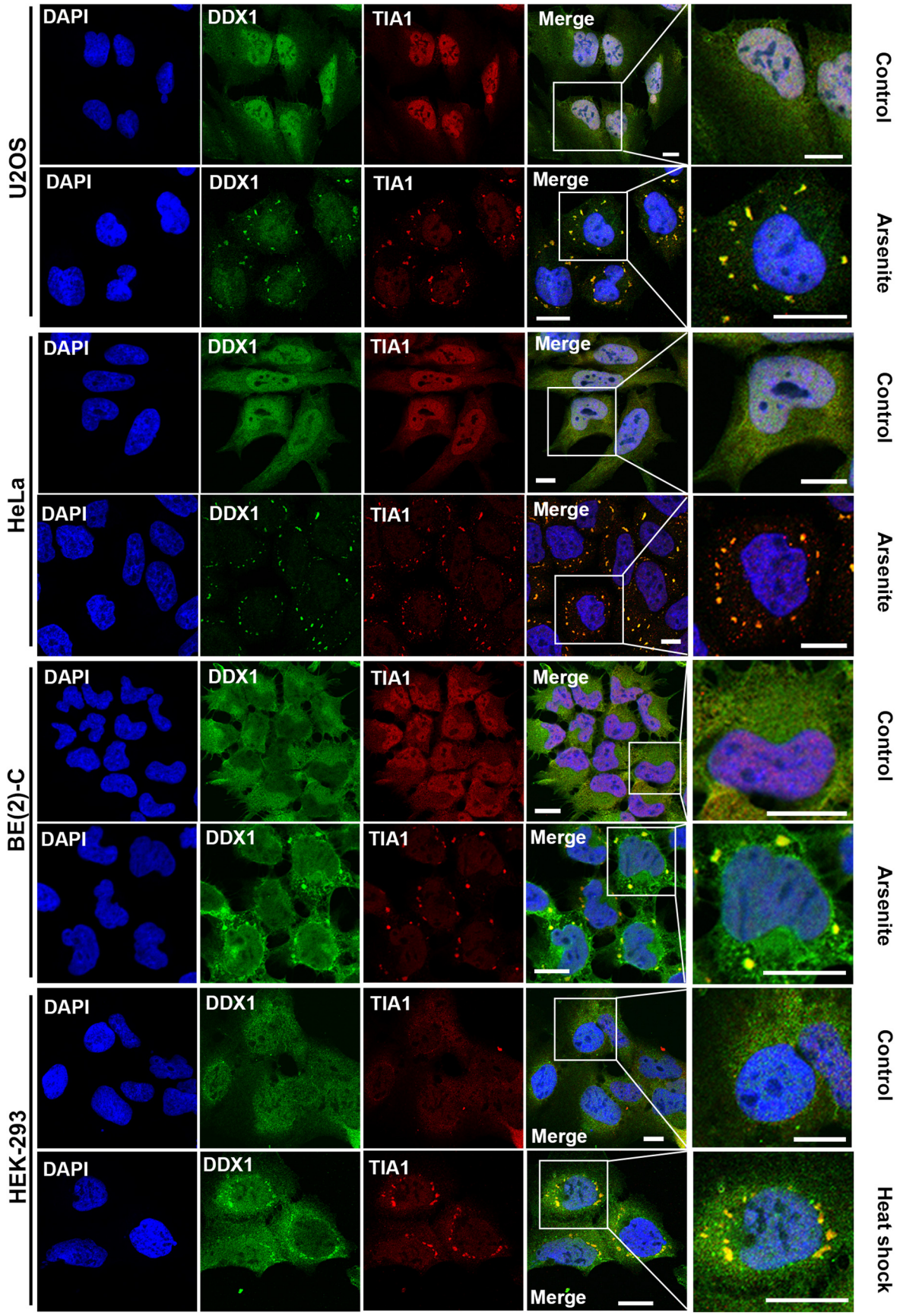

Figure 1. Localization of DDX1 in SGs in various cell lines. Cells were either left untreated (control) or treated with sodium arsenite (0.5 mM, 45 min) or heat shocked (43 °C, 40 min). Cells were then fixed and immunostained with anti-DDX1 and anti-TIA1 (marker for SG) antibodies. The areas in the squares are magnified in the panels on the right. Bars, 20 μm. DAPI, 4′,6′-diamidino-2-phenylindole; DDX1, DEAD box 1; SG, stress granule.

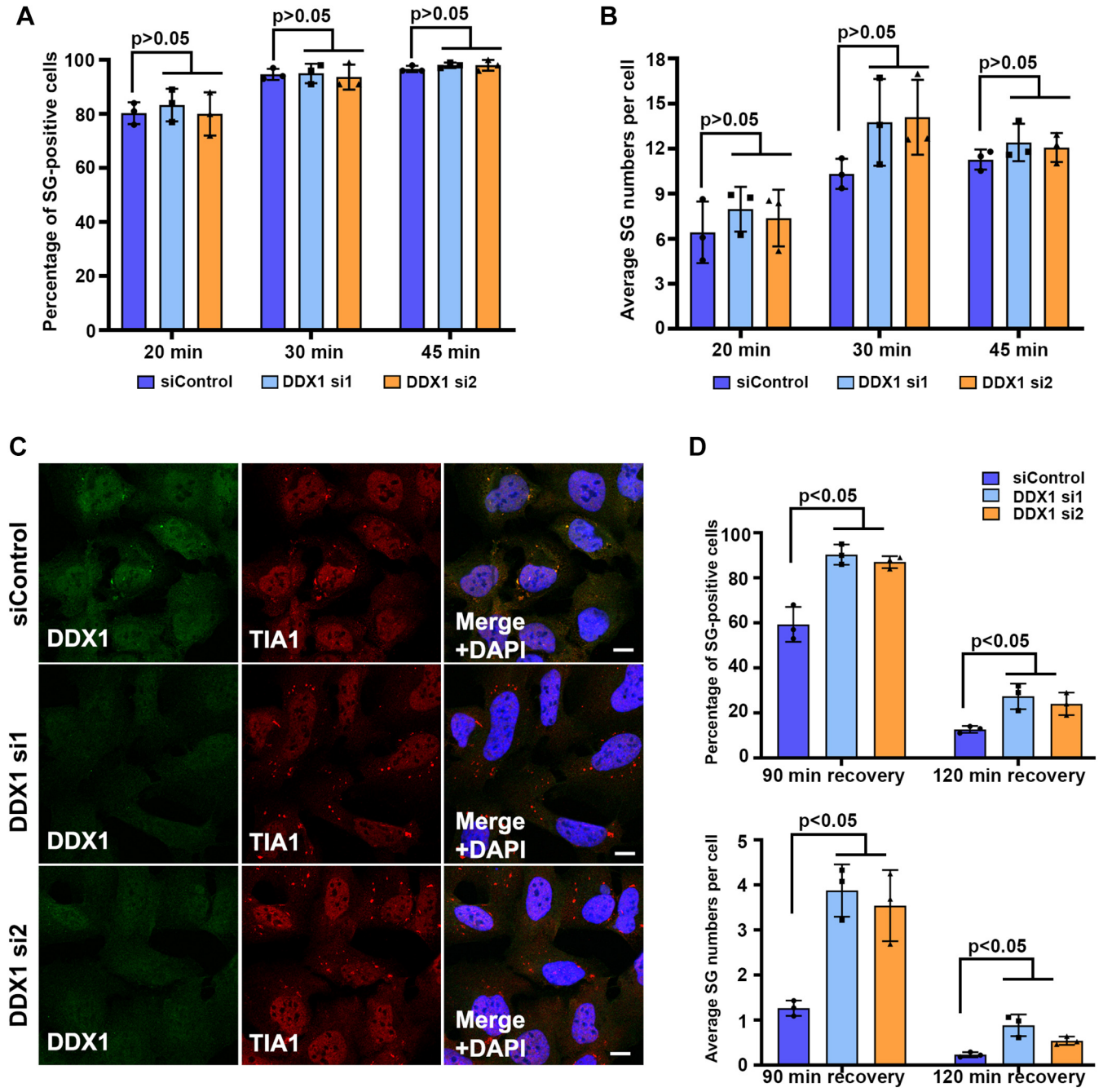

Figure 2. DDX1 facilitates SG resolution. *A* and *B*, U2OS cells were transfected with scrambled siRNA (siControl) or DDX1-specific siRNAs (si1 and si2). Forty-eight hours after transfection, cells were treated with 0.5 mM arsenite for 20, 30, or 45 min, followed by fixation and immunostaining with anti-DDX1 and anti-TIA1 antibodies. The percentage of cells positive for SG staining and the average number of SGs per cell at each time point cell are shown in (A) and (B), respectively. *C*, control or DDX1 knockdown cells were treated with 0.5 mM arsenite for 45 min. Cells were washed with warm PBS and allowed to recover in fresh medium for 90 min, followed by immunostaining with anti-DDX1 and anti-TIA1 antibodies. Bars, 10 μm. *D*, statistical analysis of cells that were positive for SG staining in control and DDX1 knockdown cells at 90 min and 120 min of recovery. For (A), (B) and (D), error bars represent standard deviation. N = 3. DDX1, DEAD box 1; SG, stress granule.

a role in SG disassembly but is dispensable for arsenite-induced SG formation and eIF2α phosphorylation/dephosphorylation.

DDX1 subcellular localization in the presence of both environmental and genotoxic stresses

We previously reported that in cells exposed to genotoxic stress, DDX1 rapidly accumulates at DNA DSBs, where it facilitates DSB repair through the homologous recombination pathway (32–34). Because cells, and especially cancer cells under treatment, may experience both environmental and genotoxic stresses, we examined DDX1 subcellular localization in cells exposed to both environmental and genotoxic stresses. First, we treated cells with both 5 Gy IR and 0.5 mM arsenite at the same time and examined DDX1 localization 60 min later. This combined treatment resulted in DDX1 localization to both DSBs (marked by γH2AX) in the nucleus and SGs

(marked by TIA1) in the cytoplasm (Fig. 3*A*). Second, we exposed cells to 5 Gy IR, allowed the cells to recover at 37 °C for 30 min and then treated the cells with 0.5 mM arsenite for 60 min. Again, DDX1 was found at both DSBs and SGs (Fig. 3*B*). Third, we treated the cells with 0.5 mM arsenite for 30 min, then immediately irradiated the cells with 5 Gy, followed by a 60 min recovery period. Interestingly, in this scenario, DDX1 was found predominantly in SGs, with ∼95% of cells showing DDX1 localization to SGs and only ∼10% of cells showing DDX1 recruitment to DSBs (Fig. 3, *C* and *E*, *F*). Fourth, we treated the cells with 0.5 mM arsenite for 30 min, washed away the drug, and allowed the cells to recover for 120 min. Cells were then irradiated with 5 Gy and immunostained 60 min later. Under these conditions, virtually all cytoplasmic SGs had resolved (Fig. 3, *D* and *E*); however, accumulation of DDX1 at DSBs was observed in ∼50% of cells (Fig. 3, *D* and *E*). The levels of DDX1 protein in the nucleus and the cytoplasm remained largely unchanged under all conditions tested (Fig. S4). These results suggest that although DDX1 plays roles in cellular responses to both environmental and genotoxic stress, pre-existing environmental stress may interfere with DDX1's response to genotoxic insult. However, this interference can be reversed.

Identification of DDX1-binding RNA targets

DDX1 is a member of the DEAD box family of RNA helicases that bind RNAs and alter their secondary structures. To identify putative mRNA targets of DDX1, we carried out triplicate RIP experiments on U2OS cells using anti-DDX1 antibody, with IgG serving as the negative control (Fig. 4*A*). DDX1-co-immunoprecipitated RNAs were reversed transcribed using random hexamers and subjected to HiSeq analysis. Approximately 30 million total reads were generated for each DDX1-IP and IgG control. Using a p-value <0.01 and a ≥10-fold read enrichment (DDX1 IP/IgG) as selection criteria, we identified 1978 genes (of a total of 27,943 reference genes) as possible targets for DDX1 (Table S1) (complete dataset can be found in Table S2). While some RNA reads were in intronic regions, most of the reads were in exonic regions and predominantly in coding regions (Fig. 4*B*). The *HSPD1* and *TDP-43* genes are shown as examples to illustrate the read coverage and enrichment in DDX1 IP and IgG controls (Fig. 4*C*). To gain insight into the biological processes with which the putative DDX1 binding RNA targets are involved, we performed gene ontology enrichment analysis of the 1978 putative target genes. Using adjusted p-values <0.01 as our standard, we found that DDX1-bound transcripts are enriched in biological processes including cellular response to stress and DNA damage response, DSB repair *via* homologous recombination, and regulation of RNA processing, localization, and stability (Fig. 4*D*).

Next, we used RT-qPCR to confirm our RIP sequencing (RIP-Seq) results on 12 selected genes: *TP53*, *ATM*, *BRCA1*, and *CtIP* (DNA DSB response and repair); *HSPD1*, *FMR1*, *FXR1*, *TAF15*, *DDX3X*, and *TDP-43* (SG components); *FAM98B* (encodes a known DDX1-interacting protein); and *SKIP* (involved in pre-mRNA splicing). In agreement with our RIP-Seq data, RT-qPCR showed significant enrichment of the selected transcripts in DDX1 RIP compared to IgG control, with eight genes showing >10-fold enrichment (*FMR1*, *BRCA*1, *HSPD1*, *FAM98B*, *TAF15*, *FXR1*, *SKIP*, and *ATM*) and four genes showing 6- to 10-fold enrichment (*CtIP*, *TP53*, *TDP-43*, and *DDX3X*) (Fig. 4*E*). We also selected four genes with similar or fewer read counts (DDX1 RIP/IgG): *PHF20*, *F2RL2*, *ZNF16*, and *OGDH* and measured their enrichment using RT-qPCR. These transcripts showed 1-4X enrichment in DDX1 RIP compared to IgG control (Fig. 4*E*). We therefore used <5-fold enrichment in RT-qPCR as a cutoff and defined the 12 mRNAs as DDX1 target RNAs and the 4 mRNAs as control RNAs.

Environmental stress enhances DDX1 binding to target RNAs

A cell under stress undergoes dramatic alterations in its protein requirements, necessitating re-allocation of post-transcriptional resources such that nonessential mRNAs are no longer translated while essential RNAs are preferentially translated (8). The role of RNA protection in these processes remains poorly understood, although it is generally accepted that RNAs that contribute to stress adaptation and are beneficial to cells during stress recovery must be preferentially preserved (12). We therefore investigated the possibility that DDX1 is protecting its target RNAs in cells exposed to environmental stress. Cells were either left untreated or treated with 0.5 mM arsenite for 45 min, and DDX1 (or IgG control) RIP carried out. Similar amounts of DDX1 were immunoprecipitated in cells cultured in either the presence or absence of arsenite (Fig. 5*A*). RNAs immunoprecipitated by anti-DDX1 antibodies were increased by 2- to 9-fold in arsenite-treated cells compared to untreated cells for eight of the 12 DDX1 target RNAs selected for analysis (*FMR1*, *BRCA1*, *CTIP*, *HSPD1*, *TP53*, *TDP-43*, *DDX3X*, and *ATM*) (Fig. 5*B*).

Arsenite is generally used to induce acute oxidative stress, whereas overnight treatment with paraquat is used to mimic chronic oxidative stress (46, 47). To see whether enhanced DDX1 binding to target RNAs is observed under different types of environmental stress, we treated U2OS cells with 10 mM paraquat for 16 h followed by DDX1-RIP and RT-qPCR analysis. Paraquat-induced stress led to >2-fold increase in the binding of DDX1 to 8 out of 12 DDX1 target RNAs, with greatly enhanced binding (>6-fold) observed for *BRCA1* and *TDP-43* (Fig. 5*C*). Again, only minimal changes were observed for control RNAs (Fig. 5*C*). Together, these results suggest that increased binding of DDX1 to its target RNAs may be a general response to oxidative stimuli.

DDX1 protects target RNAs in the cytoplasm during environmental stress

Increased binding of target RNAs to DDX1 in cells treated with arsenite and paraquat suggest the possibility that DDX1 may be playing a role in protecting a subset of cytoplasmic RNAs in stressed cells. To test this idea, we treated cells with 0.5 mM arsenite for 45 min, fractionated cells into cytoplasm

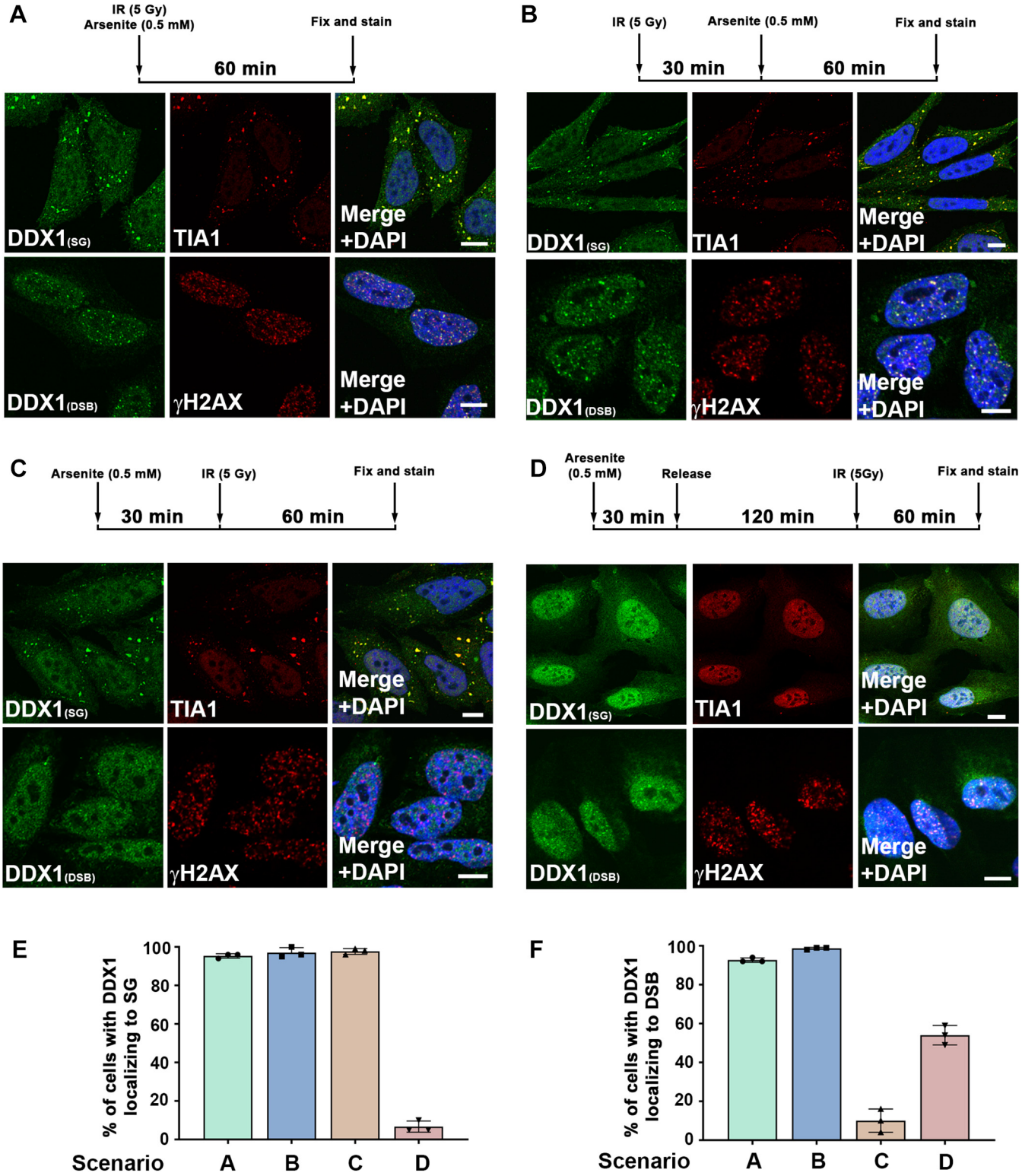

Figure 3. Cellular localization of DDX1 in the presence of genotoxic (IR) stress and environmental (arsenite) stress. HeLa cells were subjected to IR (5 Gy) and arsenite treatment (0.5 mM) concurrently (*A*), or IR first, followed by arsenite (*B*), or arsenite first, followed by IR (*C*), or arsenite first, cells allowed to recover, followed by IR (*D*). Cells were fixed and immunostained with anti-DDX1 antibody (Batch 2910, used to detect DDX1 in SGs) and anti-TIA1 antibody or anti-DDX1 antibody (Batch 2923, used to detect DDX1 at DSBs) and anti-γH2AX antibody. Bars, 10 μm. *E* and *F*, percentage of cells showing DDX1 localization to SGs (E) or DSBs (F) under the four scenarios described in (A) to (D). DDX1, DEAD box 1; DSB, double-strand break; IR, ionizing radiation; SG, stress granule.

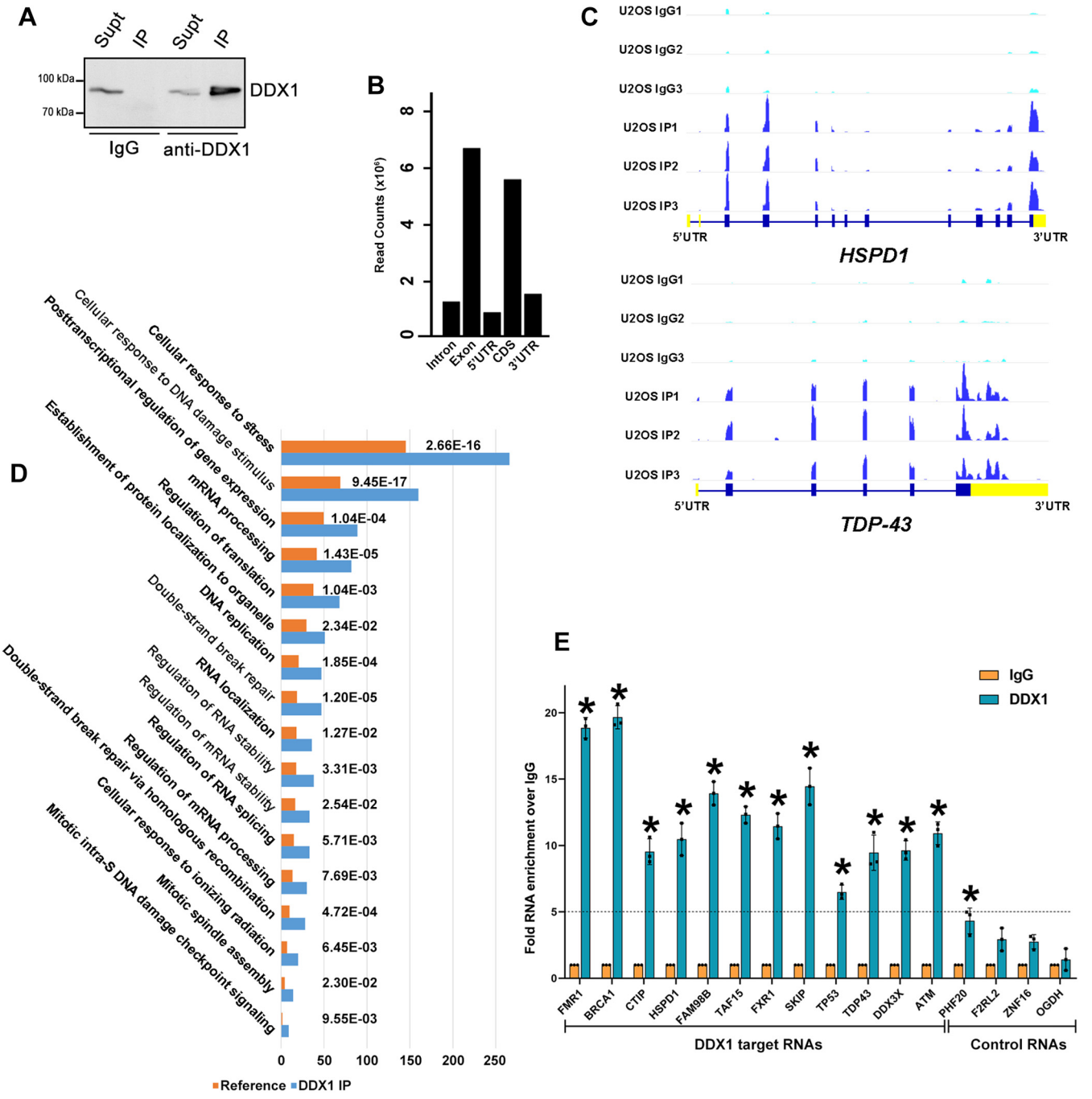

Figure 4. Identification of DDX1-bound RNAs. U2OS cells were UV-crosslinked, and whole cell lysates were prepared. Lysates were immunoprecipitated with IgG or anti-DDX1 antibody. Immunoprecipitated RNAs were extracted, reverse transcribed, and sequenced. *A*, Western blot analysis of immunoprecipitated endogenous DDX1. Eight percent of supernatant was loaded next to 50% of IP for comparison. *B*, read counts of DDX1 RIP found in introns, exons, coding sequences (CDS), and 5′- and 3′-UTRs. *C*, examples of read counts at DDX1-binding RNAs. Exons of HSPD1 and TDP-43 are shown in *thick lines* and introns are shown in *thin lines*. *Yellow color* denotes 5′- and 3′-untranslated regions (UTRs). Peaks represent the number of reads. *D*, gene ontology analysis of enriched pathways found in DDX1 RIPs. The *orange color* represents the number of genes expected if binding was random. The *blue color* denotes the actual number of genes bound by DDX1. *p*-value is shown for each category. *E*, putative DDX1 target mRNAs selected on the basis of 10X read count enrichment in DDX1 RIP-Seq *versus* IgG RIP-Seq were confirmed by RT-qPCR. Fold enrichment of transcripts in DDX1 RIPs is shown relative to IgG RIP which is set at 1. Error bars denote standard deviation. N = 3. *$p < 0.005$. DDX1, DEAD box 1; RIP, RNA immunoprecipitation; RT-qPCR, quantitative RT-PCR.

and nucleus, and compared levels of DDX1-bound RNAs in the presence or absence of stress. We found slight to moderate decreases (∼0.4–0.9) in cytoplasmic mRNA levels for all 16 genes examined (including both DDX1 targets and control RNAs) after arsenite treatment (Fig. 6*A*). We next asked whether DDX1 protects its target RNAs in the presence of stress. For this experiment, we depleted DDX1 in U2OS cells using DDX1-specific siRNAs (si1 and si2) (Fig. S5) and exposed cells to arsenite. To offset any changes that DDX1 depletion might cause at the transcriptional level, we defined the level of each DDX1 target mRNA and control mRNA as 1 in the nonstressed siControl (scrambled siRNA)-, DDX1 si1-,

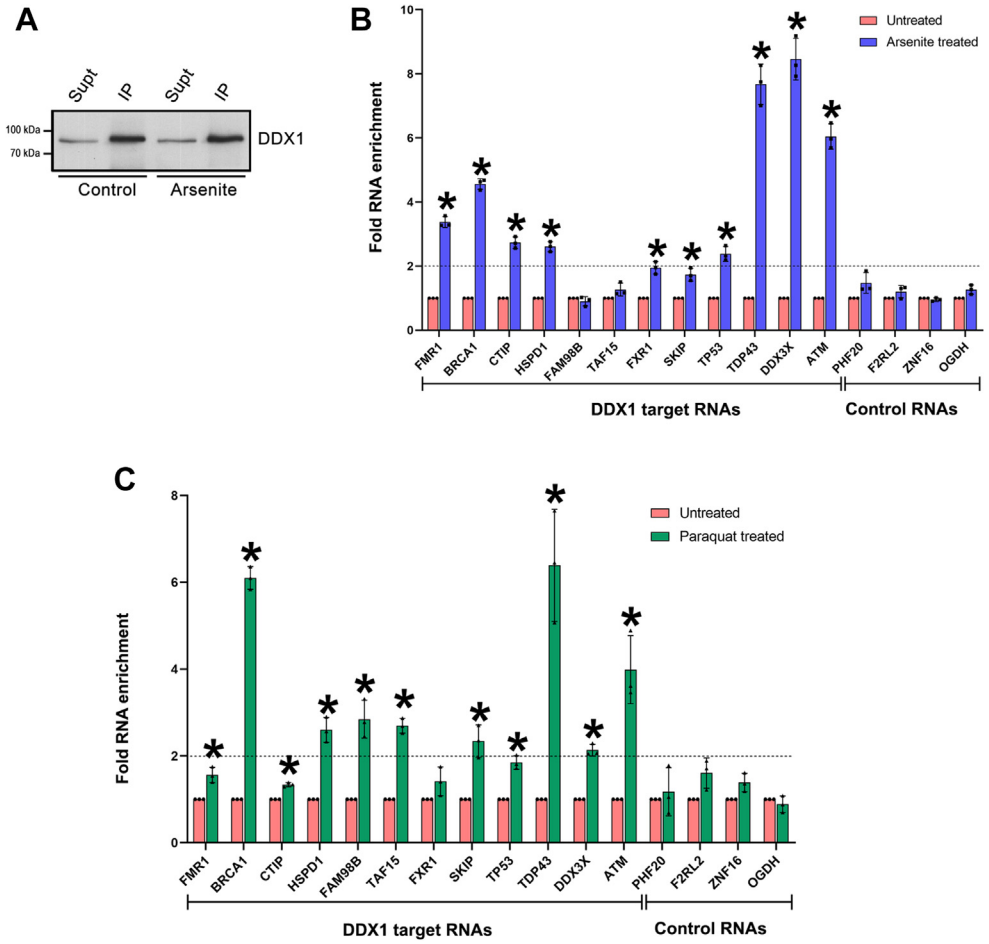

Figure 5. Enhanced binding of DDX1 to its target RNAs in arsenite- and paraquat-treated cells. *A* and *B*, U2OS cells were treated with 0.5 mM arsenite for 45 min or left untreated (control). Cells were UV-crosslinked, and whole cell lysates were generated. Lysates were immunoprecipitated with IgG or anti-DDX1 antibody. *A*, Western blot analysis of immunoprecipitated DDX1 using anti-DDX1 antibody or IgG. Eight percent of supernatant was loaded next to 40% of IP for comparison. *B*, fold enrichment of DDX1-binding RNAs in arsenite-treated *versus* untreated cells. The value of DDX1 RIP *versus* IgG RIP in untreated cells was set at 1. *C*, U2OS cells were treated with 10 mM paraquat overnight or left untreated. DDX1 RIP was performed as described above. Fold DDX1-binding RNA enrichment in paraquat-treated *versus* untreated cells was calculated as described in (B). Error bars represent standard deviation. N = 3. *$p < 0.005$. DDX1, DEAD box 1; RIP, RNA immunoprecipitation.

and DDX1 si2-transfected cells and compared DDX1 target levels in arsenite-stressed siControl-, DDX1 si1-, and DDX1 si2-transfected cells to their respective untreated counterparts set at 1 (Fig. 6). Compared to siControl-transfected cells, DDX1 si1- or si2-transfected cells showed further reductions in DDX1 target mRNA levels in the cytoplasm (Fig. 6*B*). For example, arsenite treatment resulted in an ∼2-fold (0.53) decrease in cytoplasmic *FMR1* mRNA levels compared to untreated control cells (Fig. 6*A*). That number was further reduced to 0.33 and 0.26 in arsenite-treated DDX1 si1- and DDX1 si2-transfected cells, respectively (Fig. 6*B*). In comparison, DDX1 depletion had either subtle or inconsistent effects on the levels of control mRNAs (Fig. 6*B*). Importantly, DDX1 depletion had little to no effect on DDX1 target mRNAs located in the nucleus during stress (Fig. 6*C*). Therefore, DDX1-mediated protection of its target mRNAs during stress appears to occur primarily in the cytoplasm.

As decreased levels of DDX1 target RNAs under stress could be caused by reduced stability in the absence of DDX1, we picked half (6 out of 12) of the selected DDX1 target RNAs and half (2 out of 4) of the selected control RNAs and measured mRNA decay over time in the cytoplasm of control and DDX1-depleted U2OS cells. For these experiments, novel RNA transcription was inhibited by treating cells with 5 μM actinomycin D with samples removed for RNA extraction at the 0, 1, 2, 3, and 4 h time points for both control and DDX1-depleted cells. RT-qPCR was carried out on all samples using 18S rRNA for normalization. In the absence of oxidative stress (actinomycin D treatment alone), we found that DDX1 depletion had no significant effect on the decay of both target RNAs (*ATM, BRCA1, CtIP, TDP-43, HSPD1,* and *DDX3X*) and control RNAs (*OGDH* and *F2RL2*) (Fig. S6). In contrast, when cells were treated with both actinomycin D and arsenite, knockdown of DDX1 led to significant decrease in target RNA levels, with some of them (*CtIP*, *TDP-43*, *DDX3X,* and *ATM*) showing decreases starting from 0.5 to 1 h of treatment (Fig. 7). No decrease in mRNA levels was observed for the two control RNAs *OGDH* and *F2RL2*. Collectively, our data suggest that DDX1 stabilizes its target RNAs in the cytoplasm when exposed to oxidative stress.

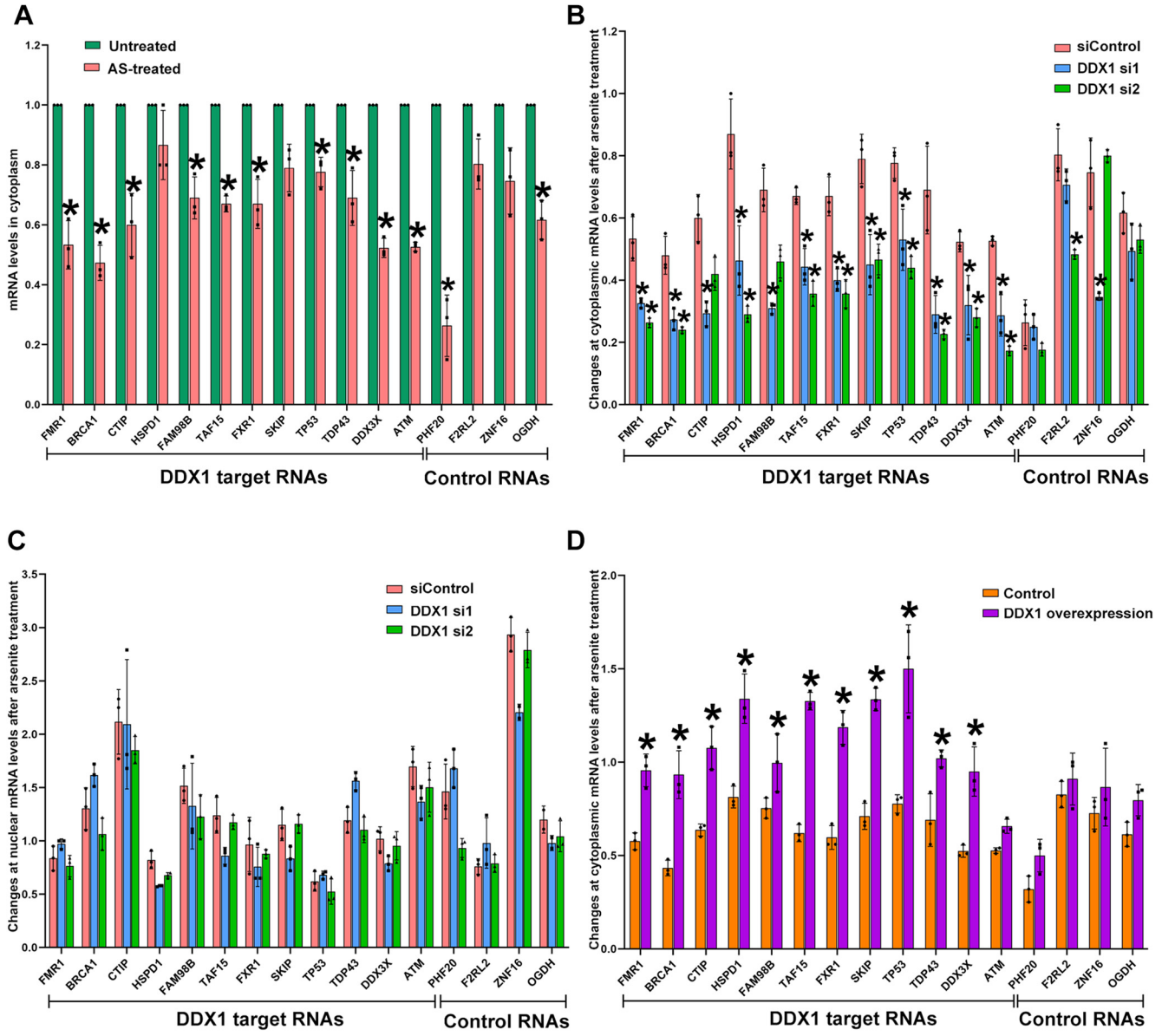

Figure 6. DDX1 is required to maintain its target mRNA levels in the cytoplasm during stress. Control and DDX1-knockdown U2OS cells were treated with arsenite or left untreated, and cytoplasmic and nuclear fractions generated. Total RNA was isolated from each fraction, reverse transcribed, and RT-qPCR was carried out to examine the levels of DDX1 targets in each fraction. *A*, relative levels of cytoplasmic DDX1 mRNA targets in arsenite-treated cells compared to untreated cells (set at 1). *B*, relative levels of cytoplasmic DDX1 mRNA targets in DDX1-depleted *versus* control cells upon arsenite treatment. Values for control arsenite-treated cells are taken from (*A*). Values for DDX1 target mRNAs in arsenite-treated siControl, DDX1 si1 and DDX1 si2 cells are relative to their respective siControl, DDX1 si1 and DDX1 si2 untreated counterparts, which were set at 1. *C*, relative levels of nuclear DDX1 mRNA targets in DDX1-depleted *versus* control cells upon arsenite treatment. Changes in nuclear mRNA levels were analyzed as described in (B). *D*, cells were transfected with GFP vector or GFP-DDX1 expression constructs. Forty-eight hours after transfection, cells were treated with arsenite and fractionated. RNA isolation, reverse transcription, and RT-qPCR quantification were performed as described above. Changes in cytoplasmic mRNA levels were analyzed as described in (B). Error bars represent standard deviation. N = 3. *$p < 0.005$. DDX1, DEAD box 1; RT-qPCR, quantitative RT-PCR.

Given the effect of DDX1 depletion on the cytoplasmic levels of its target RNAs upon arsenite treatment, we next asked whether overexpression of DDX1 might have the reverse effect. To test this, we transfected U2OS cells with a DDX1 expression construct, exposed the cells to arsenite, and examined target mRNA levels in the cytoplasm. Compared to cells transfected with empty vector, DDX1 overexpression led to significantly increased levels of DDX1 target RNAs during stress (Fig. 6*D*). This increase in mRNA levels was not observed in the case of control RNAs. Thus, the combined results from DDX1 depletion and overexpression experiments indicate that DDX1 promotes the stability of its target RNAs in the cytoplasm when cells are under oxidative stress.

Some mRNAs are stabilized within SGs during environmental stress (14, 16). We therefore asked whether DDX1 stabilizes its RNA targets in SGs following arsenite treatment by comparing the amount of target mRNA accumulating in SGs in control *versus* DDX1-depleted cells. We chose two target mRNAs for analysis, *BRCA1* and *DDX3X*, as well as one control mRNA, *GAPDH*, shown not to be bound by DDX1

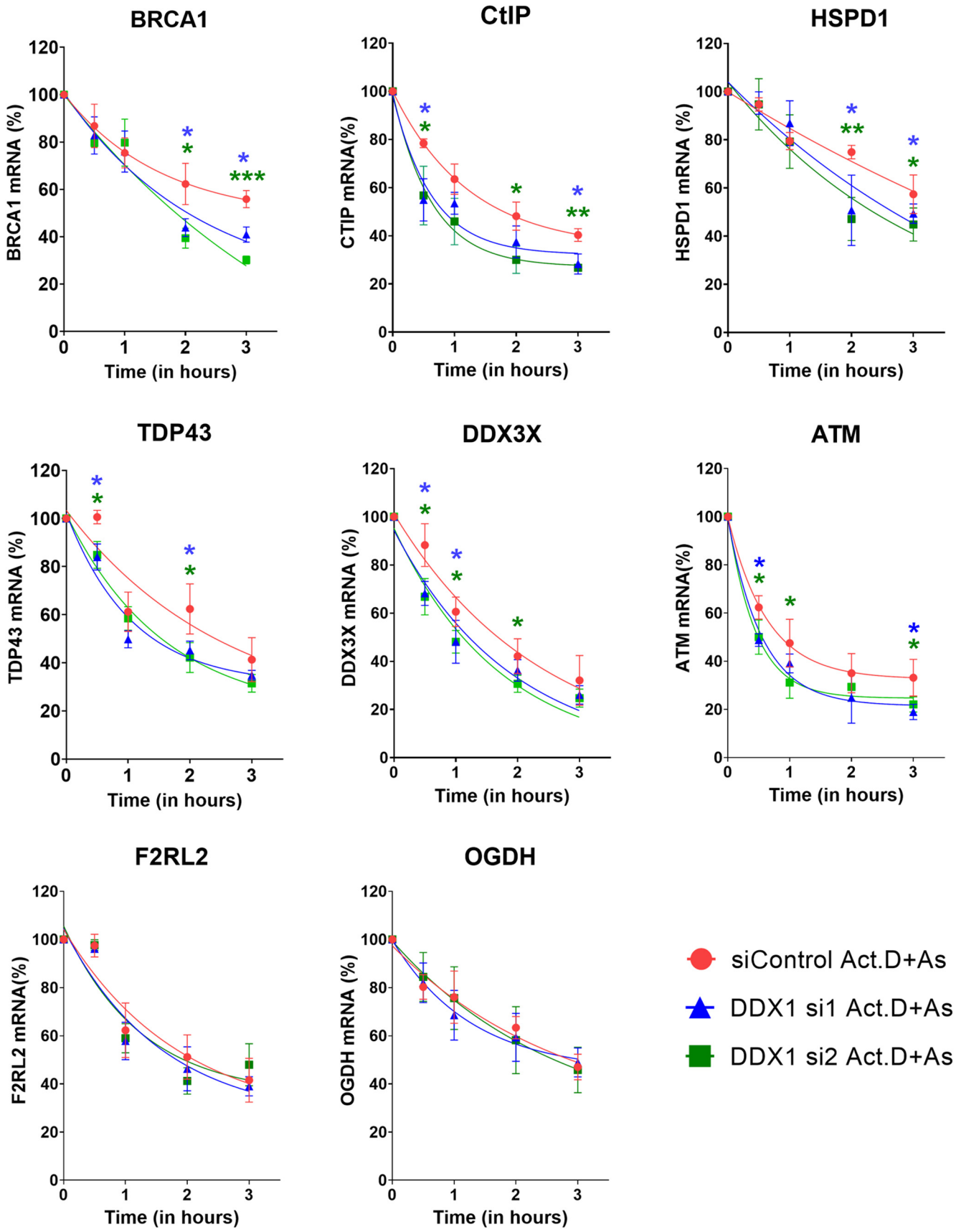

Figure 7. DDX1 depletion leads to faster target mRNA decay in the cytoplasm under stress. Control and DDX1-depleted U2OS cells were treated with both actinomycin D and arsenite for the time indicated. Cytoplasmic fractions were generated, and total RNAs were isolated. Reverse transcription was carried out using either oligod(T) (for mRNA) or random primers (for 18S RNA normalization). RT-qPCR was used to examine the levels of DDX1 target RNAs

based on our RIP-Seq experiments. mRNAs within SGs were quantified using single-molecule fluorescence *in situ* hybridization (smFISH) and SGs were visualized by anti-G3BP1 antibody immunostaining. In siControl-transfected cells, the average number of smFISH foci in SGs per cell for *BRCA1*, *DDX3* and *GAPDH* was 7.20, 10.29 and 46.32, respectively (Fig. 8), which is similar to what Khong *et al.* have previously reported (48). DDX1 depletion did not lead to significant changes in the average numbers of smFISH foci in SGs per cell for all three mRNAs (Fig. 8). The distribution of all three smFISH probes was similar throughout the cells in non-stressed control and DDX1 knockdown cells (Fig. S7). Thus, our results suggest that DDX1 may be dispensable for the accumulation of its target mRNAs in SGs with DDX1-mediated mRNA protection occurring outside SGs.

To further address our hypothesis that DDX1 protects its target mRNAs, we took advantage of the BE(2)-C NB cell line that naturally overexpresses DDX1 due to *DDX1* gene amplification (49). First, DDX1 antibody was used to immunoprecipitate DDX1-bound RNAs from control BE(2)-C cells. This was followed by RT-qPCR to check the status of the 12 target RNAs characterized in U2OS cells. These RNAs showed 6 to 30X enrichment in DDX1 RNA IPs compared to the IgG control, ranging from 6.6-fold for *TDP-43* to 35.6-fold for *ATM* (Fig. 9*A*, red columns), confirming that these RNAs are also DDX1 targets in BE(2)-C cells. Second, we tested the effect of arsenite treatment on RNA enrichment. Similar to what we observed in U2OS cells, arsenite treatment of BE(2)-C cells resulted in further increases in DDX1 binding to its target RNAs, with 10 out of 12 targets showing >2-fold enrichment compared to untreated cells (Fig. 9*A*, blue columns). Third, we investigated the effects of arsenite treatment on overall DDX1 target RNA levels in the cytoplasm of BE(2)-C cells. Compared to U2OS (shown in Fig. 6*B* and again in Fig. 9*B*, orange columns), we observed little effect on cytoplasmic DDX1 target RNAs in BE(2)-C cells, with arsenite-treated to untreated ratios ranging from 0.7 to 1.6 (Fig. 8*B*). We postulate that this difference between U2OS and BE(2)-C may be due to the naturally high levels of cytoplasmic DDX1 in BE(2)-C cells compared to U2OS cells (Fig. 9*C*). Thus, NB cells with their elevated levels of DDX1 may offer better protection of target RNAs during stress. As BE(2)-C cells are refractory to transient siRNA transfection, we generated BE(2)-C cells with stable depletion of DDX1 (Figs. 9*D* and S8) using lentivirus-based vectors. To offset any possible changes at the transcriptional level caused by DDX1 depletion, we defined the level of each DDX1 target mRNA and control mRNA as 1 in the nonstressed shControl (scrambled shRNA)-, DDX1 sh1-, and DDX1 sh2-transfected cells, as described above for U2OS cells. When exposed to arsenite, DDX1-depleted BE(2)-C cells showed significantly reduced levels of target RNAs in the cytoplasm compared to control lentivirus-transduced cells (Fig. 9*E*). Levels of control mRNAs remained largely unchanged. Taken together, these results support the idea that the naturally elevated levels of cytoplasmic DDX1 in BE(2)-C cells protect DDX1 target mRNAs during oxidative stress.

The processing body (PB) is a cytoplasmic structure enriched in enzymes required for every stage of mRNA decay (50, 51). SGs and PBs often reside adjacent to each other in stressed cells. In light of our data indicating a role for DDX1 in protecting mRNAs during stress, we examined DDX1's subcellular localization in relation to PBs. GW182, an RNA-binding protein that functions in miRNA-mediated silencing (52), was used as a marker for PBs. No colocalization was observed between DDX1 and GW182 both in the presence and absence of stress, although DDX1 (and SGs) were frequently found adjacent to PBs in arsenite-treated cells (Fig. S9).

RNA binding by DDX1 is essential for protection of its targets

It is well established that DEAD box proteins, including DDX1, bind to RNAs. To demonstrate the importance of RNA binding for the protection of DDX1 mRNA targets, we used a DDX1 mutant that is defective in binding RNAs. This DDX1 mutant, S295E/R296E/T515E/K516E (referred to as mutDDX1 henceforth), has four amino acid substitutions at the key residues that interact with substrate RNAs. mutDDX1 has previously been shown to have 100-fold lower binding affinity for RNA substrates *in vitro* compared to wildtype (wt) DDX1 (53). We generated the GFP-mutDDX1 by site-directed mutagenesis and transfected the mutant construct, or GFP-wtDDX1, into U2OS cells, followed by arsenite treatment and GFP RIP. Western blot analysis revealed similar levels of immunoprecipitated GFP-wtDDX1 and GFP-mutDDX1 in transfected cells (Fig. 10*A*). As expected, the enrichment of DDX1 target RNAs in GFP-mutDDX1 RNA-IP was drastically reduced in both the presence and absence of arsenite treatment (Fig. 10*B*), confirming that mutDDX1 fails to effectively bind target RNAs.

Next, we examined overall levels of DDX1 target RNAs in GFP-wtDDX1 and GFP-mutDDX1 transfected cells during oxidative stress. To eliminate interference by endogenous DDX1, cells were first transfected with DDX1 siRNA to deplete endogenous DDX1, followed by transfection with either GFP-wtDDX1 or GFP-mutDDX1 constructs that are resistant to DDX1 siRNA (32). We observed an increase in DDX1 mRNA target levels upon wtDDX1 overexpression (Fig. 10*C*, blue bars compared to orange graphs, significance indicated by blue asterisks). However, significantly reduced levels of target RNAs were observed in arsenite-treated GFP-mutDDX1 transfectants compared to arsenite-treated GFP-wtDDX1 transfectants (Fig. 10*C*, green bars compared to blue bars, significance indicated by green asterisks). These results indicate that RNA binding by DDX1 is required for maintenance of DDX1 target mRNA levels under stress.

Next, we tested whether binding to RNAs is required for DDX1 localization to SGs. For these experiments, we

(*BRCA1*, *CtIP*, *HSPD1*, *TDP43*, *DDX3X*, and *ATM*) or control RNAs (*F2RL2* and *OGDH*) at each time point. The percentage of residual mRNA is calculated by dividing the level of certain mRNA at a specific time point by that at time point 0 h (before treatment). *Blue* and *green asterisks* denote significant differences between siControl-transfected and DDX1 si1- or DDX1 si2-transefected cells, respectively. Error bars: standard deviation. N = 3. *$p < 0.05$, **$p < 0.005$, ***$p < 0.0005$. DDX1, DEAD box 1; RT-qPCR, quantitative RT-PCR.

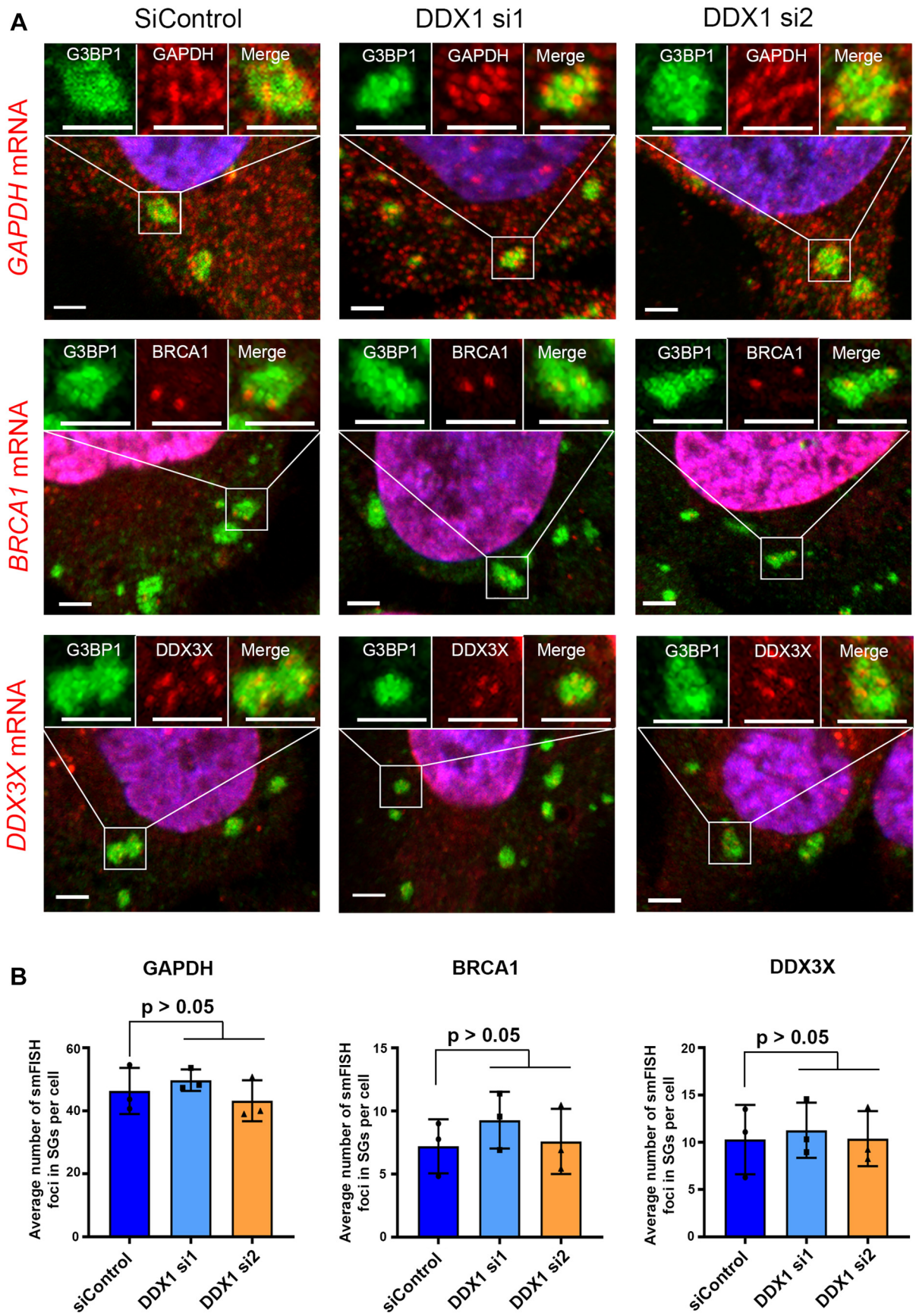

Figure 8. DDX1 is dispensable for target mRNA accumulation in SGs. U2OS cells were transfected with either scrambled siRNA (SiControl) or siRNAs specific to DDX1 (DDX1 si1 and si2). Forty-eight hours after transfection, cells were treated with 0.5 mM arsenite for 45 min and fixed with formaldehyde. *A*, cells were

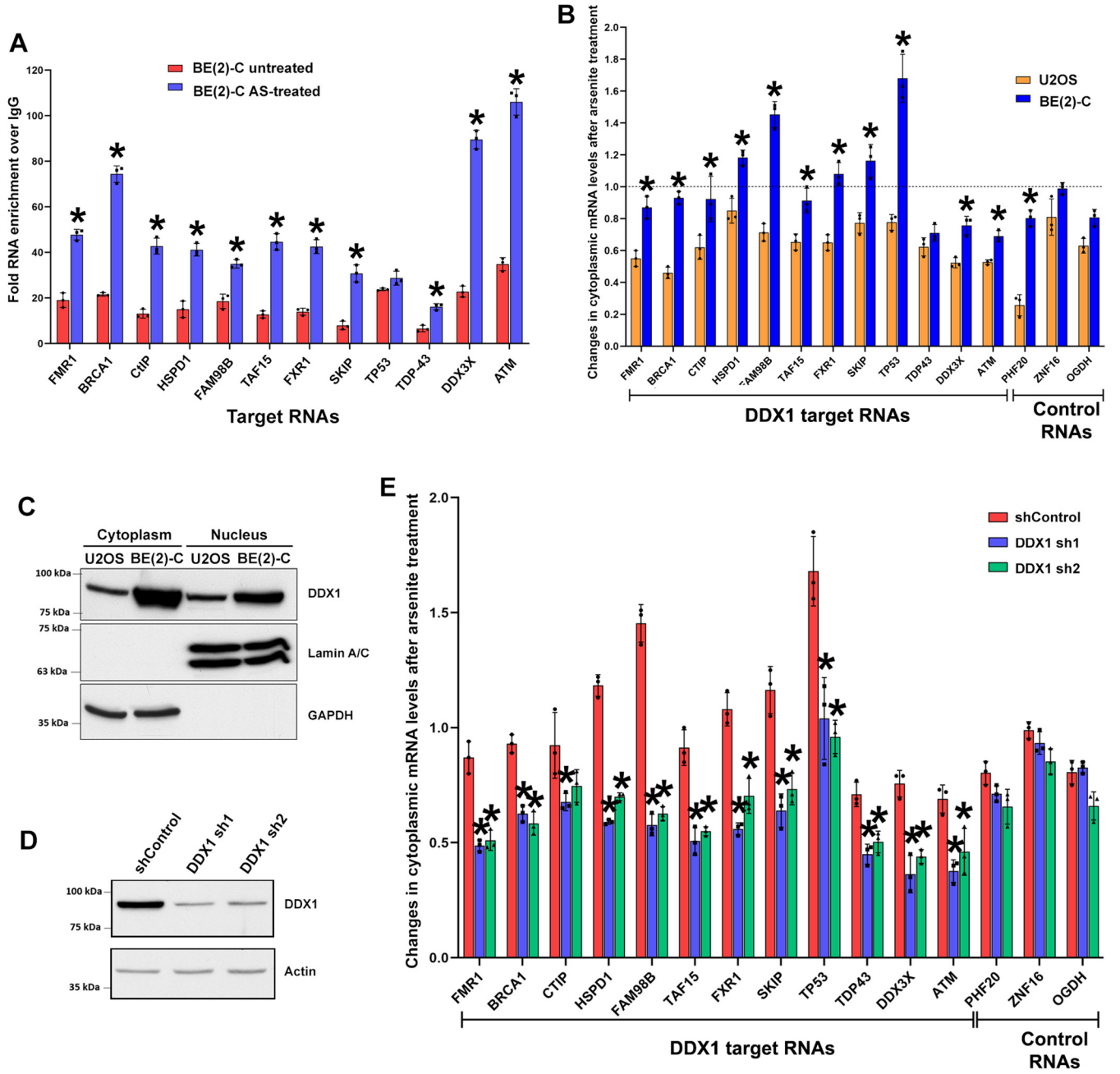

Figure 9. DDX1 protects target mRNAs in BE(2)-C cells during stress. *A*, BE(2)-C cells were treated with 0.5 mM arsenite for 45 min or left untreated. DDX1 RIP and RT-qPCR confirmation were carried out as described in Figure 4*B*. Fold enrichment for each DDX1 mRNA target in DDX1 RIP *versus* IgG RIP is shown. *B*, control and arsenite-treated U2OS and BE(2)-C cells were separated into cytoplasmic and nuclear fractions. Total RNA was isolated from cytoplasmic fractions, reverse transcribed, and quantified by RT-qPCR. Levels of DDX1 target mRNAs in arsenite-treated BE(2)-C cells are shown relative to untreated cells (set at 1). U2OS graphs from Figure 6*A* (U2OS – arsenite treated; *orange bars*) are included for comparison. Note that *F2RL2* (control RNA) is not expressed in BE(2)-C cells. *C*, Western blot analysis of cytoplasmic and nuclear fractions of U2OS and BE(2)-C cells. Lamin A/C and GAPDH served as nuclear and cytoplasmic markers, respectively. *D*, Western blot analysis showing the knockdown efficiency of DDX1 shRNAs (sh1 and sh2) in stably transfected BE(2)-C cells. *E*, changes in levels of cytoplasmic DDX1 mRNA targets in control and DDX1-depleted BE(2)-C cells after arsenite treatment. Numbers shown for arsenite-treated control, DDX1 sh1, and DDX sh2 transfectants are relative to untreated control, DDX1 sh1, and DDX1 sh2 transfectants, respectively, each of which was set at 1. Error bars represent standard deviation. N = 3. *$p < 0.005$. DDX1, DEAD box 1; RIP, RNA immunoprecipitation; RT-qPCR, quantitative RT-PCR.

transfected U2OS cells with either GFP-wtDDX1 or GFP-mutDDX1 and treated cells with arsenite. To our surprise, GFP-mutDDX1 localized to SGs (detected by the presence of the SG marker TIAR) in arsenite-treated cells, with an immunostaining pattern indistinguishable from that of GFP-wtDDX1 (Fig. 11*A*). In addition, GFP-wtDDX1 and GFP-mutDDX1 localized to SGs in virtually the same percentage of transfected cells (Fig. 11*B*). These results indicate that RNA-

hybridized with smFISH probes against *GAPDH* (control), *BRCA1*, or *DDX3X* mRNAs. SGs were visualized by anti-G3BP1 antibody immunostaining. Inserts show enlarged images of circled areas. Scale bars, 3 μm. *B*, statistical analysis of accumulation of *GAPDH*, *BRCA1*, and *DDX3X* mRNAs in SGs in control and DDX1 knockdown cells. Error bars: standard deviation. N = 3. DDX1, DEAD box 1; SG, stress granule; smFISH, single-molecule fluorescence in situ hybridization.

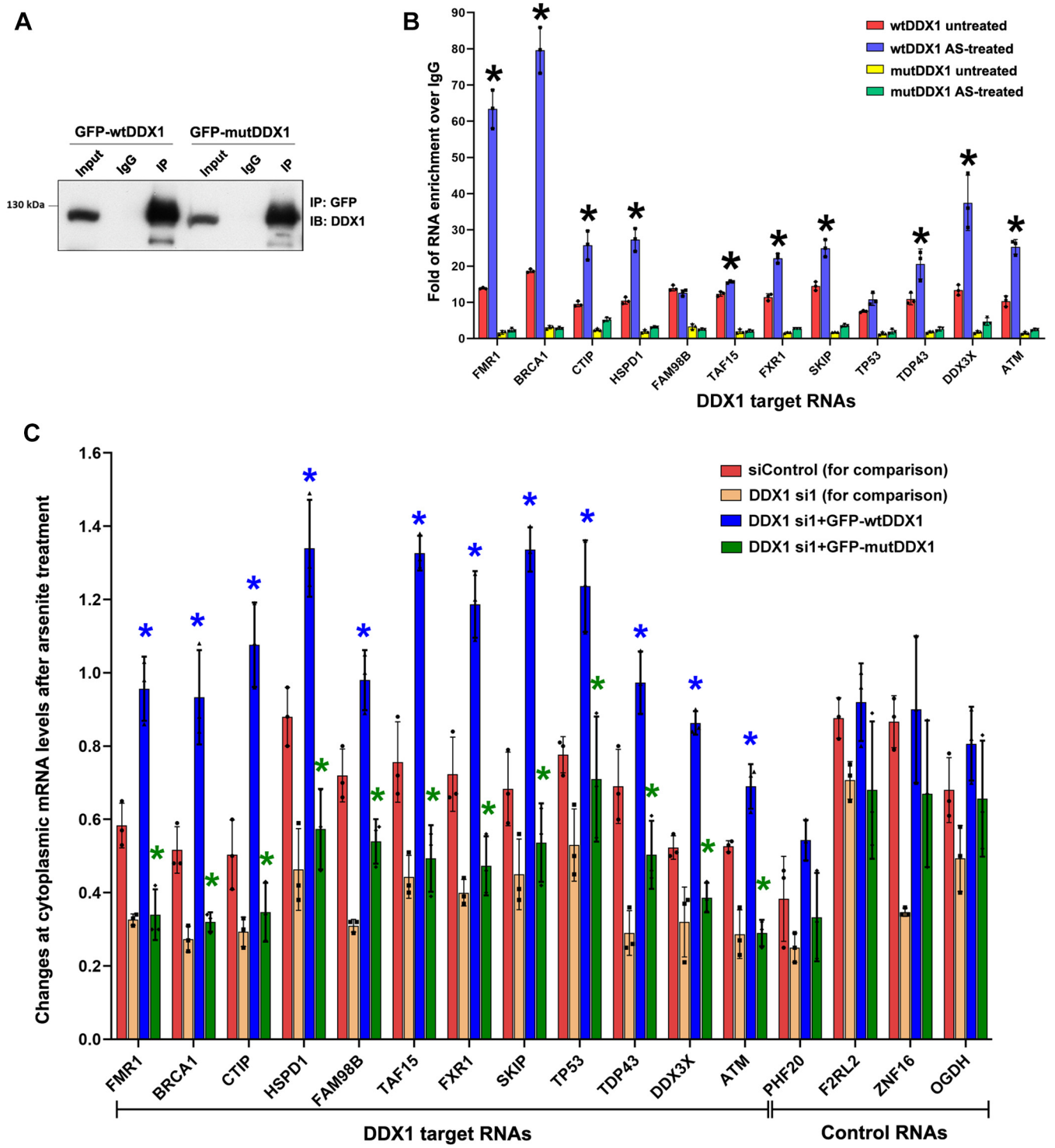

Figure 10. RNA binding is essential for protection of DDX1 target RNAs. *A* and *B*, U2OS cells were transfected with either GFP-wtDDX1 or GFP-mutDDX1. Cells were treated with 0.5 mM arsenite for 45 min or left untreated. RIP was carried out using anti-GFP antibody or IgG. *A*, Western blot analysis showing efficient IP of GFP in both GFP-wtDDX1 and GFP-mutDDX1 transfected cells. Ten percent of input was loaded next to 20% of IP for comparison. *B*, RT-qPCR analysis of DDX1 target RNAs in RIPs from control and arsenite-treated cells. Fold enrichment of target mRNAs in GFP RIP experiments is shown relative to IgG control which is set at 1 for each of the four conditions tested. *C*, DDX1-depleted cells (DDX1 si1) were transfected with either GFP-wtDDX1 or GFP- mutDDX1, treated with arsenite or left untreated, and fractionated. For comparison, scrambled siRNA (siControl)- and DDX1 si1-transfected U2OS cells were left untreated or treated with 0.5 mM arsenite for 45 min. Shown are ratios of cytoplasmic mRNA levels in arsenite-treated cells relative to untreated cells (set at 1) for siControl-transfected U2OS cells, DDX1 si1-transfected cells, GFP-wtDDX1-transfected DDX1-knockdown cells, and GFP-mutDDX1-transfected DDX1-knockdown cells. *Blue asterisks* denote significant differences compared to siControl-transfected U2OS cells. *Green asterisks* denote significant differences compared to GFP-wtDDX1 transfected cells. Error bars represent standard deviation. N = 3. *$p < 0.005$. DDX1, DEAD box 1; RIP, RNA immunoprecipitation; RT-qPCR, quantitative RT-PCR.

binding activity is dispensable for DDX1 localization to SGs. Because DDX1 facilitates SG resolution (Fig. 2), we examined whether the RNA-binding activity of DDX1 plays a role in SG disassembly during stress recovery. To eliminate interference by endogenous DDX1, we depleted endogenous DDX1 in U2OS cells with DDX1 siRNA prior to GFP-wtDDX1 and GFP-mutDDX1 transfection. We then treated the cells with arsenite and analyzed SG resolution at different time points after arsenite removal. DDX1-depleted cells transfected with empty GFP vector were used as controls for these experiments. As predicted, expression of wtDDX1 in DDX1 knockdown cells corrected the delayed SG resolution caused by DDX1-depletion (compare first and second columns at both time points, Fig. 11*C*). Results obtained with the GFP-mutDDX1 expression construct were indistinguishable from those obtained with GFP-wtDDX1 (compare second and third columns at both time points Fig. 11*C*). Together these results indicate that binding to RNAs is essential for DDX1-dependent protection of target RNAs under stress but is dispensable for both DDX1 localization to SG and DDX1-mediated SG disassembly.

Discussion

While inhibition of mRNA translation is a well-recognized hallmark of ISR, protection of cytoplasmic mRNAs during environmental stress remains poorly understood. It is known that some SG components (*e.g.*, TIA1 and IGF2BP1) transport mRNAs to SGs, and SGs contain proteins that stabilize mRNAs (*e.g.*, HuR) (13, 16, 19). Based on this evidence, it

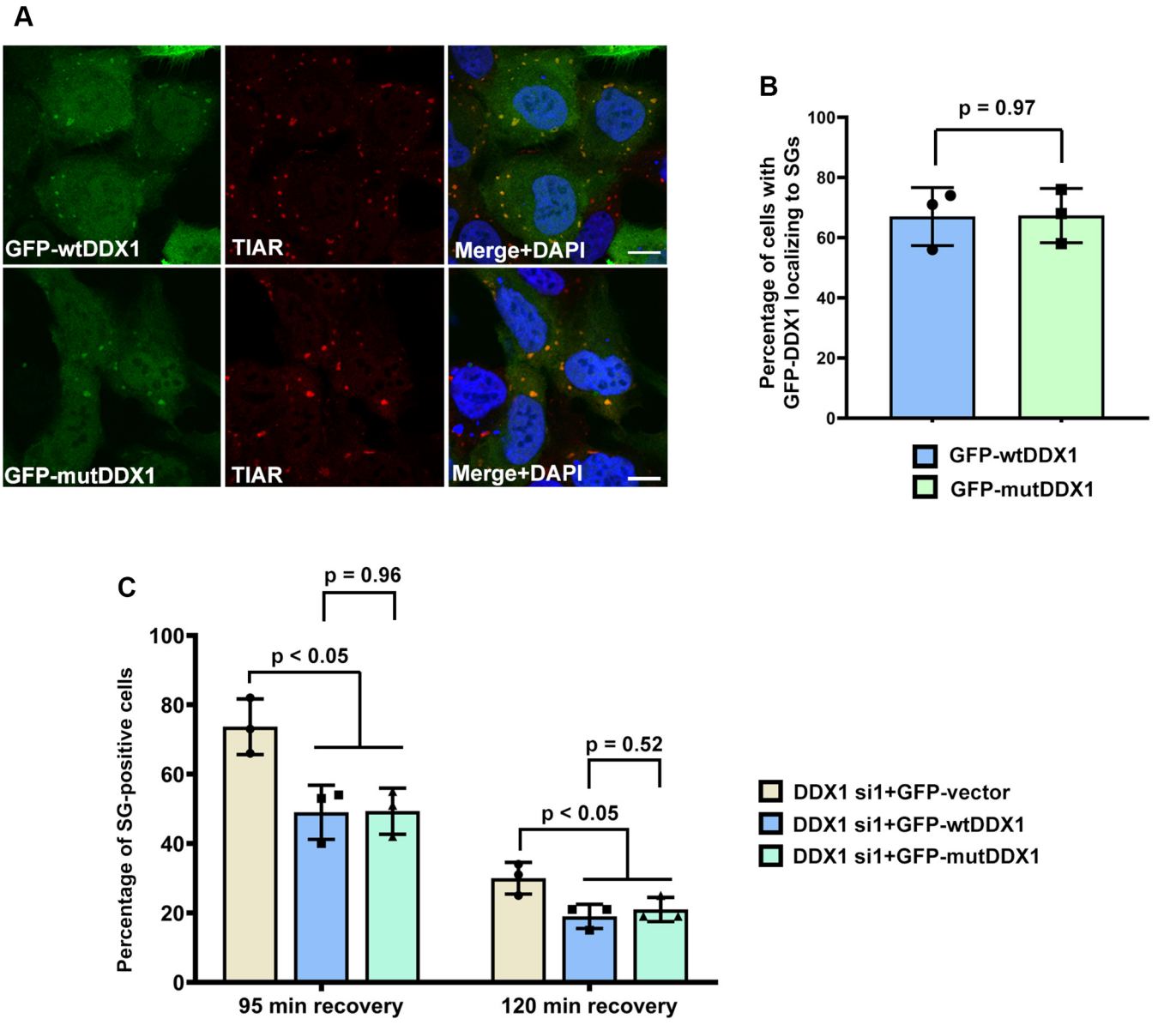

Figure 11. RNA binding is not required for DDX1 localization to SGs and SG resolution. *A*, U2OS cells transfected with GFP-wtDDX1 or GFP-mutDDX1 were treated with 0.5 mM arsenite for 45 min and immunostained with anti-TIAR antibody. Bar, 10 μm. *B*, the percentage of GFP-positive cells showing GFP-wtDDX1 or GFP-mutDDX1 localization to SGs (based on TIAR immunostaining) described in (A). *C*, cells were transfected with *DDX1*-specific siRNA (si1), followed by transfection with either GFP vector, GFP-wtDDX1 or GFP-mutDDX1. Cells were treated with 0.5 mM arsenite and allowed to recover for the indicated times. The percentage of SG-positive cells (based on TIAR immunostaining) is relative to GFP-positive cells. For (B) and (C), error bars represent standard deviation. N = 3. DDX1, DEAD box 1; SG, stress granule.

has been proposed that SGs protect key mRNAs from degradation while shunting other mRNAs to neighboring PBs where bulk mRNA is believed to be degraded based on the abundance of mRNA degradation enzymes in these structures (50, 51). However, there are reports in the literature indicating that impaired SG assembly does not influence the stability of bulk mRNA during stress in both yeast and mammalian cells (19, 20). In this study, we identify DDX1 as a new player in the oxidative stress response. We show that DDX1 is recruited to SGs generated by a variety of environmental stressors and facilitates SG resolution during recovery from oxidative stress. We identify DDX1 RNA targets and demonstrate that DDX1 protects these target RNAs under stress. Importantly, our results indicate that the RNA-binding activity of DDX1 is required for DDX1-mediated mRNA protection but is dispensable for its recruitment to SG and SG resolution. We postulate that DDX1 plays dual roles in oxidative stress response, protecting its RNA targets in the cytoplasm, a function depending on RNA binding, and interacting with its partners in SGs to facilitate cellular recovery from stress, a function independent of RNA binding.

In addition to their well-established roles in the unwinding of duplex RNAs, more recent studies have revealed that DEAD box proteins function in a much broader range of processes including ribonucleoprotein complex remodeling, RNA strand annealing/exchange, and displacement of proteins from RNAs (54). Therefore, it is not surprising that DEAD box proteins would have a role in cellular response to environmental stress. A comprehensive proteomic analysis of purified SGs identified four DDX proteins with high confidence: DDX1, DDX2 (eIF4A), DDX3X, and DDX6 (RCK/p54), along with other DDX or DExD/H box RNA helicases with lower confidence, such as DDX19A and DHX30 (5). Overexpression of DDX3X leads to SG formation even in the absence of stress (55) and cancer-associated DDX3X mutations cause SG hyperassembly (56). Hondele *et al.* reported that DDX3X (Ded1 in yeast) and DDX6 (Dhh1 in yeast) control RNA influx into and out of SGs and promote stress-induced SG assembly in an ATP-dependent manner (57). In contrast, eIF4A (DDX2), an important player in translation initiation, represses SG formation and functions as an RNA-binding chaperone that limits RNA–RNA interactions within cells (58). This function of eIF4A requires ATP-dependent RNA binding. DDX1 also has an ATPase activity that is dependent on binding with RNAs (59). We found that the RNA-binding activity of DDX1 is not required for its recruitment to SGs. Unlike eIF4A that extends from the SG core further into the shell of SGs where RNAs are enriched, DDX1 is uniformly localized within the SG core (5, 58). DDX1 has a number of properties that are different from that of other DEAD box proteins. First, DDX1 is the only DEAD box protein that contains a SPRY domain (60). Based on crystallography analysis, DDX1's SPRY domain may function independently of DEAD box proteins' RNA binding and ATPase activities (61). Second, unlike most DEAD box proteins, DDX1 binds ADP more tightly than ATP and displays stronger unwinding activity when bound to ADP (33, 62). Thus, DDX1's roles in cells under stress may depend on whether it is bound to RNA or protein, as well as availability of ADP versus ATP.

Although a number of DEAD box proteins, including DDX1, are core components of SGs, to date none has been associated with resolution of SGs. Our finding that DDX1 depletion delays SG resolution suggests a role for DDX1 in stress recovery. SG disassembly involves two steps, with the dynamic shell dissipating first, followed by resolution of the stable core (63). Players in the autophagy pathway and some chaperones have been shown to promote SG clearance (3). Given that DDX1's involvement in the resolution of arsenite-induced SG does not appear to be tied to its RNA binding activity, identification of DDX1-interacting proteins in SGs in the context of SG assembly and disassembly should provide insight into its exact role in SG resolution.

Previous reports have linked DDX1 to the binding of microRNAs and tRNAs (38, 64). However, prior to this study, no mRNA targets had been identified for DDX1. We identified 12 mRNAs bound by DDX1 in U2OS cells, with the understanding that we cannot exclude the possibility that the mRNAs enriched in our RIP-seq experiments are part of a complex that also includes RNA binding proteins other than DDX1. Further evidence that these 12 mRNAs are directly bound to DDX1 comes from the fact that these mRNAs are immunoprecipitated by the wildtype but not the RNA binding-deficient DDX1. Of these12 mRNAs, *ATM, BRCA1*, *CtIP*, and *TP53* are involved in maintaining genome stability (1), and *FMR1*, *FXR1*, *TAF15,* and *TDP-43* function in stress responses and are associated with neuronal degeneration and disorders (5, 6, 65). Importantly, DDX1 binding to its targets was increased, sometimes dramatically, when cells were exposed to either acute (arsenite) or chronic (paraquat) oxidative stress. Whether DDX1 protects/stabilizes its mRNA targets by altering their secondary structures, allowing post-transcriptional modification of RNA, and/or affecting their interactions with other RNA binding proteins remain topics of conjecture. Interestingly, arsenite treatment induces alternative polyadenylation of mRNAs (66, 67). Stress-induced alternative polyadenylation can affect mRNA stability and influence mRNA abundance during stress (66). We have previously found that DDX1 interacts with cleavage factor CSTF2 (68, 69), a factor that is essential for mRNA cleavage and regulates alternative polyadenylation (70). DDX1 has also been shown to regulate alternative splicing under stress in *Drosophila* (27, 71). It is therefore possible that DDX1 protects mRNAs that are alternatively polyadenylated during stress.

NB tumors with amplified copies of the *MYCN* gene have a poor prognosis. The *DDX1* gene is co-amplified with *MYCN* in ~50% of *MYCN*-amplified NB tumors (29, 72, 73). However, the significance of having elevated DDX1 levels in *MYCN*-amplified NB tumors remains controversial. Our discovery that DDX1 overexpression in NB cells protects RNA targets to at least to the same extent as ectopic DDX1 overexpression in U2OS cells supports a key role for DDX1 in stress responses in *DDX1*-amplified NB cells. Thus, our results may have implications for the treatment of NB patients with *DDX1*

amplification, as many chemotherapy drugs used in the clinic for cancer treatment induce stress responses and SG formation (2, 74).

Compared to nonstressed cells, more DDX1 target mRNAs are immunoprecipitated by anti-DDX1 antibody in U2OS and BE(2)-C cells under stress. At least two scenarios can account for this increase: (i) stress causes more DDX1 molecules to bind to its target mRNAs. For example, as a result of stress-induced global suppression of translation, ribosomes are released from mRNAs undergoing translation. This may lead to increased amounts of mRNAs with more accessible binding sites for DDX1 and (ii) DDX1 binds to its target mRNAs with greater affinity during stress. We were not able to distinguish between these two possibilities, because although approximately equal amounts of DDX1 was immunoprecipitated in the presence and absence of stress, it was not possible to determine what portion of the precipitated DDX1 actually binds to mRNAs. Nevertheless, both scenarios underscore the importance of forming stable mRNP complexes (in this case mRNA-DDX1) for mRNA protection during stress, as previously proposed for other RNA binding proteins such as IGF2BP1 (14, 19).

The fact that the RNA-binding activity of DDX1 is required for protecting its target RNAs but not for recruitment to SGs suggests dual roles for DDX1 in the cellular stress response. Our results showing that DDX1 knockdown does not affect the SG localization of two mRNAs (*BRCA1* and *DDX3X*) normally found in SGs further suggest that DDX1 is not required for the localization of its target mRNAs to SGs. Thus, DDX1-mediated mRNA protection may occur outside of SGs. In agreement with this, recent studies show that although most mRNAs can accumulate in SGs with variable efficiencies, SGs only contain ∼10% of cytoplasmic mRNAs (21, 48). Furthermore, SG localization does not appear to affect mRNA translation or decay compared to their mRNA counterparts that remain in the cytosol during stress (21, 22). Therefore, our findings support the idea that mRNA protection during stress is independent of SG assembly. However, SGs may still serve as hubs for regulation of signaling pathways and post-translational RNA modifications under stress conditions (75, 76). Thus, SG formation and cytoplasmic mRNA protection in stressed cells may represent separate but important parts of the prosurvival homeostatic response to environmental stress.

In conclusion, we show that DDX1 is recruited to SGs in cells exposed to a variety of environmental stressors, including heat shock, ER stressor thapsigargin, proteasome inhibitor MG132 as well as acute and chronic oxidative stress. DDX1 facilitates SG resolution during recovery from oxidative stress. We demonstrate that DDX1 binds to and protects its target mRNAs from degradation in the cytoplasm of cells undergoing oxidative stress. We report that DDX1 binding to its RNA targets, while critical for RNA protection, is dispensable for DDX1 recruitment to SGs. These results, when combined with DDX1's previously demonstrated roles in genotoxic stress responses and the inability to generate DDX1 knockout cells (25, 26, 37), suggest that DDX1 is an important modulator of stress responses that promotes cell adaptation under stress.

Experimental procedures

Cells and treatments

HeLa (cervical cancer), U2OS (osteosarcoma), and BE(2)-C (NB) cells were cultured in DMEM supplemented with 10% fetal calf serum, 100 U/ml penicillin, and 100 μg/ml streptomycin. For arsenite treatment, cells were incubated with 0.5 mM sodium arsenite (Sigma-Aldrich, S7400) for the specified times. For paraquat treatment, cells were treated with 10 mM paraquat (Sigma-Aldrich, 856,177) for 16 h. Other types of stress conditions included 43 °C for 40 min (heat shock); 1 mM H_2O_2 for 120 min (oxidative stress); 10 μM MG132 (Sigma-Aldrich, M7449) for 60 min (proteasome stress); and 2 μM thapsigargin (Sigma-Aldrich, T9033) for 60 min (endoplasmic reticulum stress). For ionizing radiation exposure, cells were γ-irradiated using a Shepherd ^{137}Cs irradiator and allowed to recover at 37 °C for the specified times prior to analysis.

Constructs and transfections

To generate the S295E/R296E/T515E/K516E DDX1 mutant that is defective in RNA binding (53), base substitutions resulting in changes at the designated amino acids were introduced using the QuikChange site-directed mutagenesis protocol (Agilent Technologies). The same protocol was used to generate the GFP-wtDDX1 and GFP-mutDDX1 (RNA-binding defective) constructs that are resistant to DDX1 siRNA1 (si1) as described previously (32). All constructs were sequenced to ensure that there were no unwanted mutations. Constructs were transfected into cells using polyethylenimine (Polysciences Inc) at a ratio of 5 μg reagent to 1 μg DNA. Arsenite treatment was carried out 48 h posttransfection unless otherwise stated.

Fluorescence microscopy

Cells cultured on coverslips were fixed and processed as previously described (32, 33). Two rabbit anti-DDX1 antibodies made in house (batch 2910 and 2923; 1:1000 dilution unless otherwise stated) were used in this study. Both antibodies were generated using the N terminus of DDX1 (amino acids 1–186) (49, 68). Batch 2910 is preferentially used for Western blot analysis, DDX1 immunoprecipitation, and detection of DDX1 in SGs (33, 34, 49, 68). Batch 2923 is used for detection of DDX1 at DNA DSBs (32–34). Other antibodies include mouse anti-G3BP1 (1:400, BD Biosciences, 611126), human anti-GW182 (1:1000, a gift from Dr Marvin Fritzler, University of Calgary), mouse anti-γ-H2AX (1:4000; EMD Millipore, 05–636), goat anti-TIA1 (1:400, Santa Cruz Biotechnologies, SC-1751), and goat anti-TIAR (1:400, Santa Cruz Biotechnologies, SC-1749). Coverslips were mounted onto slides in polyvinyl alcohol (Calbiochem)-based mounting medium containing 1 μg/ml 4′,6′-diamidino-2-phenylindole (DAPI). Images were acquired using a Zeiss LM710 confocal microscope, exported as TIFF files using ZEN, and assembled

using Photoshop software. To quantify cells that are positive for SG staining during stress or stress recovery, confocal microscopy images were randomly captured, and cells that were positive for SG staining were scored.

For SG quantification, confocal microscope images were captured and analyzed with the "Spot" module of Imaris Image Analysis Software (Version 9.9.0, Bitplane AG, Switzerland). SGs and cell nuclei were identified based on anti-TIA1 antibody and DAPI staining, respectively. All images were background subtracted. Estimated diameter was set above 0.8 μm, and quality was set above 4500. The same parameters were applied to all images taken from the same experiment to obtain the total number of SGs in each image. The average number of SGs per cell was calculated by dividing the total number of SGs by the total number of cells (nuclei) within the same image. Approximately 100 to 150 cells were analyzed for each condition tested in each experiment, with each experiment carried out three times. Graphs were generated in Prism 8 (GraphPad). The *p*-value was calculated using the two-sided Student's *t* test.

DDX1 knockdown by siRNAs and shRNAs

DDX1 was knocked-down in U2OS cells using two different siRNAs: DDX1 si1 (CAGGCUGAAUCUAUCCCAUUGAUCU) and DDX1 si2 (UACACCAUGUUGUU GUCCCAGUAAA). Scrambled siRNAs (medium GC and low GC negative controls) served as negative controls. All siRNAs including scrambled controls were purchased from ThermoFisher Scientific. Transfection of siRNAs was carried out with Lipofectamine RNAiMAX (ThermoFisher Scientific) at a final siRNA concentration of 10 nM. To obtain maximum depletion of DDX1, cells were passaged 48 h after the first round of siRNA transfection and underwent a second round of siRNA transfections. Cells were analyzed 48 h after the second round of transfection. Because BE(2)-C cells are refractory to siRNA transfection, DDX1 depletion in BE(2)-C cells was by transduction of lentiviruses that carry MISSION pLKo.1 shRNAs (Millipore Sigma) specific to *DDX1*. The two shRNA sequences used in this study were: DDX1 sh-1 (CCGGCCGGGCAATCAAGGAACATAACTCGAGTTATGTTCCTTGATTGCCCGGTTTTTG) and DDX1 sh-2 (CCGGGCATGGGTGTAGAGCTACTAACTCGAGTTAGTAGCTCTACACCCATGCTTTTTG). MISSION pLKo.1 shRNA control plasmid (shc002) was used as a negative control. Stable transfectants were selected in DMEM medium containing 2 μg/ml puromycin. Successful knockdown was confirmed by Western blotting using anti-DDX1 antibody (batch 2910, 1:5000) on whole cell lysates.

RNA immunoprecipitation

U2OS and BE(2)-C cells at 80 to 90% confluency were either treated with 0.5 mM sodium arsenite for 45 min or left untreated. Crosslinking was carried out using a UV Crosslinker (VWR Canada) at 200 mJ/cm^2. Whole cell lysates were prepared by resuspending cells in lysis buffer [50 mM Tris-HCl pH 7.5, 150 mM NaCl, 0.5% NP-40, 0.5% deoxycholate, 5 mM EDTA, 2 mM DTT, 0.5 unit/μl RNase inhibitor (ThermoFisher Scientific) and 1X Complete protease inhibitors (Roche)]. Cell lysates were rotated for 10 min at 4 °C, followed by centrifugation at 15,000 rpm for 10 min at 4 °C to remove insoluble debris. Supernatants were collected and stored at −80 °C until use. Approximately 500 μg of supernatants were incubated with IgG or anti-DDX1 antibody (batch 2910) for 2 h at 4 °C, followed by incubation with Protein A beads (GE Healthcare) for 1 h. Immunoprecipitates were washed five times in wash buffer (50 mM Tris-HCl pH 7.5, 1% NP-40, 1% deoxycholate, 1 M NaCl and 5 mM EDTA), followed by DNase buffer (40 mM Tris-HCl pH 8.0, 10 mM $MgSO_4$, 1 mM $CaCl_2$). Beads were then incubated with Turbo DNase (12 units; ThermoFisher Scientific) for 30 min at 37 °C, followed by Proteinase K (Roche) digestion for 30 min at 37 °C. RNAs were extracted using a neutral pH phenol:-chloroform (1:1) mixture followed by ethanol precipitation and resuspension in RNase-free H_2O. RIP-Seq was carried out using triplicate samples. In Figure 9, RIP was carried out using mouse anti-GFP (clone GF28R) antibody (ThermoFisher Scientific) with mouse IgG serving as control.

HiSeq analysis and identification of DDX1 targets

Immunoprecipitated RNAs were reverse transcribed with random hexamers, and libraries were prepared using the QIAseq FX single cell RNA library kit (QIAGEN) following the manufacturer's instructions. Pair-ended sequencing was done at MedGenome Inc. using the Illumina HiSeq platform. The sequencing data were aligned with STAR aligner using human reference genome hg19 provided by CLIPSeqTools (77). The read counts per nucleotide on each exon were obtained from CLIPSeqTools, and upper quantile normalizations were performed with preprocessCore (Preprocesscore: A Collection of Pre-Processing Functions. R package version 1.58.0; https://github.com/bmbolstad/preprocessCore). *p*-value of each gene was obtained by equal variance *t* test. Genes with $p < 0.01$ and a ≥10-fold read enrichment (DDX1 IP/IgG) were selected.

Whole cell lysates, cell fractionation, RNA extraction, and Western blot analysis

Whole cell lysates were prepared as described previously (32, 34). 50 μg of lysates were resolved on SDS-PAGE gels, transferred to nitrocellulose membranes, and immunoblotted with anti-DDX1 (batch 2910, 1:5000) and anti-actin (Millipore Sigma, A3854, 1:20,000) antibodies. Nuclear and cytoplasmic fractions were generated using the protocol described by Díaz-Muñoz *et al.* (78) with modifications. Briefly, cells were harvested and incubated in cytoplasmic lysis buffer (25 mM Tris-HCl pH 7.5, 10 mM NaCl, 2.5 mM $MgCl_2$, 0.5% NP-40, 2 mM EDTA, 2 mM DTT, 0.2 unit/μl RNase inhibitor, and 1X Complete protease inhibitors) for 5 min at 4 °C, vortexed at medium setting for 5 s, and kept on ice for 1 min. The lysate was centrifuged at 1500 rpm for 5 min, with the supernatant serving as the cytoplasmic fraction. For the nuclear fraction, the pellet was incubated in nuclear lysis buffer (50 mM Tris-HCl pH 7.5, 150 mM NaCl, 1% NP-40, 0.5% deoxycholate,

5 mM EDTA, 2 mM DTT, 0.2 unit/μl RNase inhibitor, and 1X complete protease inhibitors) for 5 min at 4 °C, centrifuged at 15,000 rpm for 10 min, and the supernatant collected. Total RNAs from the cytoplasmic and nuclear fractions were extracted using Trizol LS (ThermoFisher Scientific) and resuspended in RNase-free H_2O. Reverse transcription was carried out with oligo d(T) and SuperScript II reverse transcriptase. To evaluate the purity of the cytoplasmic and nuclear fractions, 20 μg of each fraction were separated by SDS-PAGE, transferred to membranes, and immunoblotted with anti-DDX1 (batch 2910, 1:5000), anti-α-tubulin (Developmental Studies Hybridoma Bank, 12G10, 1:1000), anti-GAPDH (ThermoFisher Scientific, MA5-15738, 1:2000) (cytoplasmic marker), or anti-laminA/C (ThermoFisher Scientific, mab636, 1:500) (nuclear marker) antibodies.

Quantitative PCR analysis

RT-qPCR was carried out with SYBR green-based qPCR MasterMix-R (Applied Biological Materials Inc) following the manufacturer's instructions and analyzed on an ABI 7900HT PCR system (Applied Biosystems). Reverse transcription of immunoprecipitated RNAs was carried out using random hexamers or oligo(dT), with similar results obtained in both cases. Fold changes were calculated using the $2^{-(\Delta\Delta Ct)}$ method, and *GAPDH* mRNA was used for normalizing. To measure enhanced binding of DDX1 to target RNAs after arsenite or paraquat treatment, target RNA enrichment in DDX1 RNA-IP was normalized based on individual mRNA levels after treatment. Each experiment was done at least three times. The *p*-value was calculated using the two-sided Student's *t* test. Sequences of primers used in analysis are listed in Table S3.

Measurement of cytoplasmic mRNA decay

Control and DDX1-depleted U2OS cells were treated with 5 μM actinomycin D (Sigma-Aldrich, A9415) to inhibit RNA transcription for 0.5, 1, 2, 3, or 4 h or left untreated (0 h). Cytoplasmic fractions were generated as described above. Total RNAs were prepared using Trizol (ThermoFisher Scientific) and resuspended in RNase-free H_2O. Reverse transcription was carried out using oligo(dT), and RT-qPCR was carried out using gene-specific primers (Table S3) as described above. Target mRNA levels at each time point were normalized using 18S rRNA (reverse transcribed with random hexamers). The percentage of the remaining target mRNAs at each time point compared to untreated samples were plotted over time. To measure the cytoplasmic mRNA turnover under oxidative stress, cells were treated with 5 μM actinomycin D and 0.5 mM sodium arsenite for 0.5, 1, 2, or 3 h. Four hours treatment was not included due to > 50% cell death observed at that time point. All experiment were done in triplicates.

Immunofluorescence and RNA smFISH

Custom Stellaris smFISH probes were designed for *BRCA1* (NM_007294) and *DDX3X* (NM_001193416) using the Stellaris RNA FISH Probe Designer (available online at https://www.biosearchtech.com/stellaris-designer). Sequences of probe sets are listed in Table S4. *BRCA1* and *DDX3X* probe sets were labeled with CALFluor Red 590 and purchased from LGC Biosearch Technologies together with the predesigned smFISH probe set against *GAPDH* (SMF-2026).

Control or DDX1-depleted U2OS cells were either treated with 0.5 mM arsenite for 45 min or left untreated. Cells were then fixed and hybridized with the smFISH probes against *BRCA1*, *DDX3X*, or *GAPDH* following the manufacturer's protocol (https://biosearchassets.blob.core.windows.net/assets/bti_custom_stellaris_immunofluorescence_protocol.pdf). SGs were immunostained with mouse anti-G3BP1 antibody. Images were acquired using a Zeiss LM710 confocal microscope with a 63X objective lens and analyzed using the Imaris Image Analysis Software (Version 9.9.0, Bitplane AG). To quantify the number of smFISH foci for specific mRNAs found in SGs, images were first processed with a 3X3X1 median filter under the "Surpass" module to reduce background noise. Using the "Colocalization" module, smFISH foci that colocalize with G3BP1 staining were then selected. To exclude the smFISH signal that colocalize with G3BP1 in the nucleus, a mask that covers the nuclei was generated under the "Surface" module based on DAPI staining. Any colocalization between smFISH probes and G3BP1 within this mask was excluded from further analysis. Finally, the number of smFISH foci that localized within SGs was determined using the "Cell" module. To eliminate any effect on smFISH quantification of altered cytoplasmic mRNA levels in DDX1 knockdown cells, smFISH foci numbers of target mRNA were normalized against its cytoplasmic mRNA levels as determined by RT-qPCR. The average number of smFISH foci in SGs per cell was calculated by dividing the total number of smFISH foci that colocalize with SGs by the total number of cells analyzed. Approximately 20 to 30 cells were analyzed for each condition tested in each experiment, with each experiment carried out three times. The *p*-value was calculated using the two-sided Student's *t* test.

Data availability

The raw data for the RIP-Seq analysis of U2OS cells have been deposited in the Sequence Read Archive (National Institutes of Health) under BioProject: PRJNA784310. Sequencing data can be accessed in SRR17055941, SRR17055940, SRR17055939, SRR17055938, SRR17055937, SRR17055936.

Supporting information—This article contains supporting information.

Acknowledgments—We are grateful to Ms Tracy Jordan and Dr Gane Ka-Shu Wong for help with next generation sequencing. We thank Dr Marvin Fritzler, University of Calgary, for the anti-GW182 antibody.

Author contribution—L. L., M. G., and R. G. conceptualization; L. L., M. G., Y. W., W. W. methodology; L. L. and M. G. investigation; L. L. and M. G. validation; L. L. and R. G. writing-original draft, L. L., M. G., Y. W., W. W., and R. G. writing-review & editing; Y. W.

software; Y. W. formal analysis; Y. W. data curation; R. G. supervision; R. G. project administration; R. G. funding acquisition.

Funding and additional information—This work was supported by a grant from the Canadian Institutes of Health Research, Canada—grant number 162157.

Conflict of interest—The authors declare that they have no conflicts of interest with the contents of this article.

Abbreviations:—The abbreviations used are: DDX1, DEAD Box 1; DSB, double-strand break; IR, ionizing radiation; ISR, integrated stress response; NB, neuroblastoma; PB, processing body; RIP-seq, RNA immunoprecipitation sequencing; SG, stress granule; smFISH, single-molecule fluorescence *in situ* hybridization.

References

1. Ciccia, A., and Elledge, S. J. (2010) The DNA damage response: making it safe to play with knives. *Mol. Cell* **40**, 179–204
2. Anderson, P., Kedersha, N., and Ivanov, P. (2015) Stress granules, P-bodies and cancer. *Biochim. Biophys. Acta* **1849**, 861–870
3. Hofmann, S., Kedersha, N., Anderson, P., and Ivanov, P. (2021) Molecular mechanisms of stress granule assembly and disassembly. *Biochim. Biophys. Acta Mol. Cell Res.* **1868**, 118876
4. Protter, D. S. W., and Parker, R. (2016) Principles and properties of stress granules. *Trends Cell Biol.* **26**, 668–679
5. Jain, S., Wheeler, J. R., Walters, R. W., Agrawal, A., Barsic, A., and Parker, R. (2016) ATPase-modulated stress granules contain a diverse proteome and substructure. *Cell* **164**, 487–498
6. Wolozin, B., and Ivanov, P. (2019) Stress granules and neurodegeneration. *Nat. Rev. Neurosci.* **20**, 649–666
7. Ramaswami, M., Taylor, J. P., and Parker, R. (2013) Altered ribostasis: RNA-protein granules in degenerative disorders. *Cell* **154**, 727–736
8. Pakos-Zebrucka, K., Koryga, I., Mnich, K., Ljujic, M., Samali, A., and Gorman, A. M. (2016) The integrated stress response. *EMBO Rep.* **17**, 1374–1395
9. Donnelly, N., Gorman, A. M., Gupta, S., and Samali, A. (2013) The eIF2alpha kinases: their structures and functions. *Cell Mol. Life Sci.* **70**, 3493–3511
10. Jackson, R. J., Hellen, C. U., and Pestova, T. V. (2010) The mechanism of eukaryotic translation initiation and principles of its regulation. *Nat. Rev. Mol. Cell Biol.* **11**, 113–127
11. Mazroui, R., Sukarieh, R., Bordeleau, M. E., Kaufman, R. J., Northcote, P., Tanaka, J., *et al.* (2006) Inhibition of ribosome recruitment induces stress granule formation independently of eukaryotic initiation factor 2alpha phosphorylation. *Mol. Biol. Cell* **17**, 4212–4219
12. Anderson, P., and Kedersha, N. (2008) Stress granules: the Tao of RNA triage. *Trends Biochem. Sci.* **33**, 141–150
13. Kedersha, N. L., Gupta, M., Li, W., Miller, I., and Anderson, P. (1999) RNA-binding proteins TIA-1 and TIAR link the phosphorylation of eIF-2 alpha to the assembly of mammalian stress granules. *J. Cell Biol.* **147**, 1431–1442
14. Stohr, N., Lederer, M., Reinke, C., Meyer, S., Hatzfeld, M., Singer, R. H., *et al.* (2006) ZBP1 regulates mRNA stability during cellular stress. *J. Cell Biol.* **175**, 527–534
15. Kedersha, N., Cho, M. R., Li, W., Yacono, P. W., Chen, S., Gilks, N., *et al.* (2000) Dynamic shuttling of TIA-1 accompanies the recruitment of mRNA to mammalian stress granules. *J. Cell Biol.* **151**, 1257–1268
16. Kedersha, N., and Anderson, P. (2002) Stress granules: sites of mRNA triage that regulate mRNA stability and translatability. *Biochem. Soc. Trans.* **30**, 963–969
17. Gowrishankar, G., Winzen, R., Dittrich-Breiholz, O., Redich, N., Kracht, M., and Holtmann, H. (2006) Inhibition of mRNA deadenylation and degradation by different types of cell stress. *Biol. Chem.* **387**, 323–327
18. Hilgers, V., Teixeira, D., and Parker, R. (2006) Translation-independent inhibition of mRNA deadenylation during stress in Saccharomyces cerevisiae. *RNA* **12**, 1835–1845
19. Bley, N., Lederer, M., Pfalz, B., Reinke, C., Fuchs, T., Glass, M., *et al.* (2015) Stress granules are dispensable for mRNA stabilization during cellular stress. *Nucl. Acids Res.* **43**, e26
20. Buchan, J. R., Muhlrad, D., and Parker, R. (2008) P bodies promote stress granule assembly in Saccharomyces cerevisiae. *J. Cell Biol.* **183**, 441–455
21. Wilbertz, J. H., Voigt, F., Horvathova, I., Roth, G., Zhan, Y., and Chao, J. A. (2019) Single-molecule imaging of mRNA localization and regulation during the integrated stress response. *Mol. Cell* **73**, 946–958.e7
22. Mateju, D., Eichenberger, B., Voigt, F., Eglinger, J., Roth, G., and Chao, J. A. (2020) Single-molecule imaging reveals translation of mRNAs localized to stress granules. *Cell* **183**, 1801–1812.e13
23. Horvathova, I., Voigt, F., Kotrys, A. V., Zhan, Y., Artus-Revel, C. G., Eglinger, J., *et al.* (2017) The dynamics of mRNA turnover revealed by single-molecule imaging in single cells. *Mol. Cell* **68**, 615–625.e9
24. Linder, P., and Jankowsky, E. (2011) From unwinding to clamping - the DEAD box RNA helicase family. *Nat. Rev. Mol. Cell Biol.* **12**, 505–516
25. Hildebrandt, M. R., Germain, D. R., Monckton, E. A., Brun, M., and Godbout, R. (2015) Ddx1 knockout results in transgenerational wild-type lethality in mice. *Sci. Rep.* **5**, 9829
26. Hildebrandt, M. R., Wang, Y., Li, L., Yasmin, L., Glubrecht, D. D., and Godbout, R. (2019) Cytoplasmic aggregation of DDX1 in developing embryos: early embryonic lethality associated with Ddx1 knockout. *Dev. Biol.* **455**, 420–433
27. Germain, D. R., Li, L., Hildebrandt, M. R., Simmonds, A. J., Hughes, S. C., and Godbout, R. (2015) Loss of the Drosophila melanogaster DEAD box protein Ddx1 leads to reduced size and aberrant gametogenesis. *Dev. Biol.* **407**, 232–245
28. Godbout, R., and Squire, J. (1993) Amplification of a DEAD box protein gene in retinoblastoma cell lines. *Proc. Natl. Acad. Sci. U. S. A.* **90**, 7578–7582
29. Squire, J. A., Thorner, P. S., Weitzman, S., Maggi, J. D., Dirks, P., Doyle, J., *et al.* (1995) Co-amplification of MYCN and a DEAD box gene (DDX1) in primary neuroblastoma. *Oncogene* **10**, 1417–1422
30. Germain, D. R., Graham, K., Glubrecht, D. D., Hugh, J. C., Mackey, J. R., and Godbout, R. (2011) DEAD box 1: a novel and independent prognostic marker for early recurrence in breast cancer. *Breast Cancer Res. Treat.* **127**, 53–63
31. Boonsawat, P., Joset, P., Steindl, K., Oneda, B., Gogoll, L., Azzarello-Burri, S., *et al.* (2019) Elucidation of the phenotypic spectrum and genetic landscape in primary and secondary microcephaly. *Genet. Med.* **21**, 2043–2058
32. Li, L., Germain, D. R., Poon, H. Y., Hildebrandt, M. R., Monckton, E. A., McDonald, D., *et al.* (2016) DEAD box 1 facilitates removal of RNA and homologous recombination at DNA double-strand breaks. *Mol. Cell Biol.* **36**, 2794–2810
33. Li, L., Monckton, E. A., and Godbout, R. (2008) A role for DEAD box 1 at DNA double-strand breaks. *Mol. Cell Biol.* **28**, 6413–6425
34. Li, L., Poon, H. Y., Hildebrandt, M. R., Monckton, E. A., Germain, D. R., Fahlman, R. P., *et al.* (2017) Role for RIF1-interacting partner DDX1 in BLM recruitment to DNA double-strand breaks. *DNA Repair (Amst)* **55**, 47–63
35. Kanai, Y., Dohmae, N., and Hirokawa, N. (2004) Kinesin transports RNA: isolation and characterization of an RNA-transporting granule. *Neuron* **43**, 513–525
36. Miller, L. C., Blandford, V., McAdam, R., Sanchez-Carbente, M. R., Badeaux, F., DesGroseillers, L., *et al.* (2009) Combinations of DEAD box proteins distinguish distinct types of RNA: Protein complexes in neurons. *Mol. Cell Neurosci.* **40**, 485–495
37. Ribeiro de Almeida, C., Dhir, S., Dhir, A., Moghaddam, A. E., Sattentau, Q., Meinhart, A., *et al.* (2018) RNA helicase DDX1 converts RNA G-quadruplex structures into R-loops to promote IgH class switch recombination. *Mol. Cell* **70**, 650–662.e8
38. Popow, J., Jurkin, J., Schleiffer, A., and Martinez, J. (2014) Analysis of orthologous groups reveals archease and DDX1 as tRNA splicing factors. *Nature* **511**, 104–107

39. Suzuki, T., Katada, E., Mizuoka, Y., Takagi, S., Kazuki, Y., Oshimura, M., *et al.* (2021) A novel all-in-one conditional knockout system uncovered an essential role of DDX1 in ribosomal RNA processing. *Nucl. Acids Res.* **49**, e40
40. Li, Z., Zhou, M., Cai, Z., Liu, H., Zhong, W., Hao, Q., *et al.* (2018) RNA-binding protein DDX1 is responsible for fatty acid-mediated repression of insulin translation. *Nucl. Acids Res.* **46**, 12052–12066
41. Chen, H. C., Lin, W. C., Tsay, Y. G., Lee, S. C., and Chang, C. J. (2002) An RNA helicase, DDX1, interacting with poly(A) RNA and heterogeneous nuclear ribonucleoprotein K. *J. Biol. Chem.* **277**, 40403–40409
42. Ozeki, K., Sugiyama, M., Akter, K. A., Nishiwaki, K., Asano-Inami, E., and Senga, T. (2019) FAM98A is localized to stress granules and associates with multiple stress granule-localized proteins. *Mol. Cell Biochem.* **451**, 107–115
43. Kunde, S. A., Musante, L., Grimme, A., Fischer, U., Muller, E., Wanker, E. E., *et al.* (2011) The X-chromosome-linked intellectual disability protein PQBP1 is a component of neuronal RNA granules and regulates the appearance of stress granules. *Hum. Mol. Genet.* **20**, 4916–4931
44. Onishi, H., Kino, Y., Morita, T., Futai, E., Sasagawa, N., and Ishiura, S. (2008) MBNL1 associates with YB-1 in cytoplasmic stress granules. *J. Neurosci. Res.* **86**, 1994–2002
45. Aulas, A., Stabile, S., and Vande Velde, C. (2012) Endogenous TDP-43, but not FUS, contributes to stress granule assembly *via* G3BP. *Mol. Neurodegener* **7**, 54
46. Meyerowitz, J., Parker, S. J., Vella, L. J., Ng, D., Price, K. A., Liddell, J. R., *et al.* (2011) C-Jun N-terminal kinase controls TDP-43 accumulation in stress granules induced by oxidative stress. *Mol. Neurodegener* **6**, 57
47. Manning-Bog, A. B., McCormack, A. L., Li, J., Uversky, V. N., Fink, A. L., and Di Monte, D. A. (2002) The herbicide paraquat causes up-regulation and aggregation of alpha-synuclein in mice: paraquat and alpha-synuclein. *J. Biol. Chem.* **277**, 1641–1644
48. Khong, A., Matheny, T., Jain, S., Mitchell, S. F., Wheeler, J. R., and Parker, R. (2017) The stress granule transcriptome reveals principles of mRNA accumulation in stress granules. *Mol. Cell* **68**, 808–820.e5
49. Godbout, R., Packer, M., and Bie, W. (1998) Overexpression of a DEAD box protein (DDX1) in neuroblastoma and retinoblastoma cell lines. *J. Biol. Chem.* **273**, 21161–21168
50. Anderson, P., and Kedersha, N. (2006) RNA granules. *J. Cell Biol.* **172**, 803–808
51. Decker, C. J., and Parker, R. (2012) P-Bodies and stress granules: possible roles in the control of translation and mRNA degradation. *Cold Spring Harb. Perspect. Biol.* **4**, a012286
52. Jakymiw, A., Lian, S., Eystathioy, T., Li, S., Satoh, M., Hamel, J. C., *et al.* (2005) Disruption of GW bodies impairs mammalian RNA interference. *Nat. Cell Biol.* **7**, 1267–1274
53. Lamichhane, R., Hammond, J. A., Pauszek, R. F., 3rd, Anderson, R. M., Pedron, I., van der Schans, E., *et al.* (2017) A DEAD-box protein acts through RNA to promote HIV-1 Rev-RRE assembly. *Nucl. Acids Res.* **45**, 4632–4641
54. Valentini, M., and Linder, P. (2021) Happy birthday: 30 Years of RNA helicases. *Methods Mol. Biol.* **2209**, 17–34
55. Lai, M. C., Lee, Y. H., and Tarn, W. Y. (2008) The DEAD-box RNA helicase DDX3 associates with export messenger ribonucleoproteins as well as tip-associated protein and participates in translational control. *Mol. Biol. Cell* **19**, 3847–3858
56. Valentin-Vega, Y. A., Wang, Y. D., Parker, M., Patmore, D. M., Kanagaraj, A., Moore, J., *et al.* (2016) Cancer-associated DDX3X mutations drive stress granule assembly and impair global translation. *Sci. Rep.* **6**, 25996
57. Hondele, M., Sachdev, R., Heinrich, S., Wang, J., Vallotton, P., Fontoura, B. M. A., *et al.* (2019) DEAD-box ATPases are global regulators of phase-separated organelles. *Nature* **573**, 144–148
58. Tauber, D., Tauber, G., Khong, A., Van Treeck, B., Pelletier, J., and Parker, R. (2020) Modulation of RNA condensation by the DEAD-box protein eIF4A. *Cell* **180**, 411–426.e16
59. Edgcomb, S. P., Carmel, A. B., Naji, S., Ambrus-Aikelin, G., Reyes, J. R., Saphire, A. C., *et al.* (2012) DDX1 is an RNA-dependent ATPase involved in HIV-1 Rev function and virus replication. *J. Mol. Biol.* **415**, 61–74
60. Godbout, R., Li, L., Liu, R. Z., and Roy, K. (2007) Role of DEAD box 1 in retinoblastoma and neuroblastoma. *Future Oncol.* **3**, 575–587
61. Kellner, J. N., and Meinhart, A. (2015) Structure of the SPRY domain of the human RNA helicase DDX1, a putative interaction platform within a DEAD-box protein. *Acta Crystallogr. F Struct. Biol. Commun.* **71**, 1176–1188
62. Kellner, J. N., Reinstein, J., and Meinhart, A. (2015) Synergistic effects of ATP and RNA binding to human DEAD-box protein DDX1. *Nucl. Acids Res.* **43**, 2813–2828
63. Wheeler, J. R., Matheny, T., Jain, S., Abrisch, R., and Parker, R. (2016) Distinct stages in stress granule assembly and disassembly. *Elife* **5**, e18413
64. Han, C., Liu, Y., Wan, G., Choi, H. J., Zhao, L., Ivan, C., *et al.* (2014) The RNA-binding protein DDX1 promotes primary microRNA maturation and inhibits ovarian tumor progression. *Cell Rep.* **8**, 1447–1460
65. Crawford, D. C., Acuna, J. M., and Sherman, S. L. (2001) FMR1 and the fragile X syndrome: Human genome epidemiology review. *Genet. Med.* **3**, 359–371
66. Zheng, D., Wang, R., Ding, Q., Wang, T., Xie, B., Wei, L., *et al.* (2018) Cellular stress alters 3'UTR landscape through alternative polyadenylation and isoform-specific degradation. *Nat. Commun.* **9**, 2268
67. Hollerer, I., Curk, T., Haase, B., Benes, V., Hauer, C., Neu-Yilik, G., *et al.* (2016) The differential expression of alternatively polyadenylated transcripts is a common stress-induced response mechanism that modulates mammalian mRNA expression in a quantitative and qualitative fashion. *RNA* **22**, 1441–1453
68. Bleoo, S., Sun, X., Hendzel, M. J., Rowe, J. M., Packer, M., and Godbout, R. (2001) Association of human DEAD box protein DDX1 with a cleavage stimulation factor involved in 3'-end processing of pre-MRNA. *Mol. Biol. Cell* **12**, 3046–3059
69. Li, L., Roy, K., Katyal, S., Sun, X., Bleoo, S., and Godbout, R. (2006) Dynamic nature of cleavage bodies and their spatial relationship to DDX1 bodies, Cajal bodies, and gems. *Mol. Biol. Cell* **17**, 1126–1140
70. Grozdanov, P. N., Masoumzadeh, E., Kalscheuer, V. M., Bienvenu, T., Billuart, P., Delrue, M. A., *et al.* (2020) A missense mutation in the CSTF2 gene that impairs the function of the RNA recognition motif and causes defects in 3' end processing is associated with intellectual disability in humans. *Nucl. Acids Res.* **48**, 9804–9821
71. Van Vranken, J. G., Bricker, D. K., Dephoure, N., Gygi, S. P., Cox, J. E., Thummel, C. S., *et al.* (2014) SDHAF4 promotes mitochondrial succinate dehydrogenase activity and prevents neurodegeneration. *Cell Metab.* **20**, 241–252
72. Manohar, C. F., Salwen, H. R., Brodeur, G. M., and Cohn, S. L. (1995) Co-amplification and concomitant high levels of expression of a DEAD box gene with MYCN in human neuroblastoma. *Genes Chromosomes Cancer* **14**, 196–203
73. George, R. E., Kenyon, R. M., McGuckin, A. G., Malcolm, A. J., Pearson, A. D., and Lunec, J. (1996) Investigation of co-amplification of the candidate genes ornithine decarboxylase, ribonucleotide reductase, syndecan-1 and a DEAD box gene, DDX1, with N-myc in neuroblastoma. United Kingdom Children's Cancer Study Group. *Oncogene* **12**, 1583–1587
74. Mahboubi, H., and Stochaj, U. (2017) Cytoplasmic stress granules: dynamic modulators of cell signaling and disease. *Biochim. Biophys. Acta Mol. Basis Dis.* **1863**, 884–895
75. Kedersha, N., Ivanov, P., and Anderson, P. (2013) Stress granules and cell signaling: more than just a passing phase? *Trends Biochem. Sci.* **38**, 494–506
76. Hofweber, M., and Dormann, D. (2019) Friend or foe-Post-translational modifications as regulators of phase separation and RNP granule dynamics. *J. Biol. Chem.* **294**, 7137–7150
77. Maragkakis, M., Alexiou, P., Nakaya, T., and Mourelatos, Z. (2016) CLIP-SeqTools–a novel bioinformatics CLIP-seq analysis suite. *RNA* **22**, 1–9
78. Diaz-Munoz, M. D., Kiselev, V. Y., Le Novere, N., Curk, T., Ule, J., and Turner, M. (2017) Tia1 dependent regulation of mRNA subcellular location and translation controls p53 expression in B cells. *Nat. Commun.* **8**, 530